Journal of Electrical and Computer Engineering

Evolutionary, Neural and Fuzzy Systems for Smart and Micro Grids

Lead Guest Editor: Alessandro Niccolai
Guest Editors: Mohamed Louzazni and Alfredo Nespoli

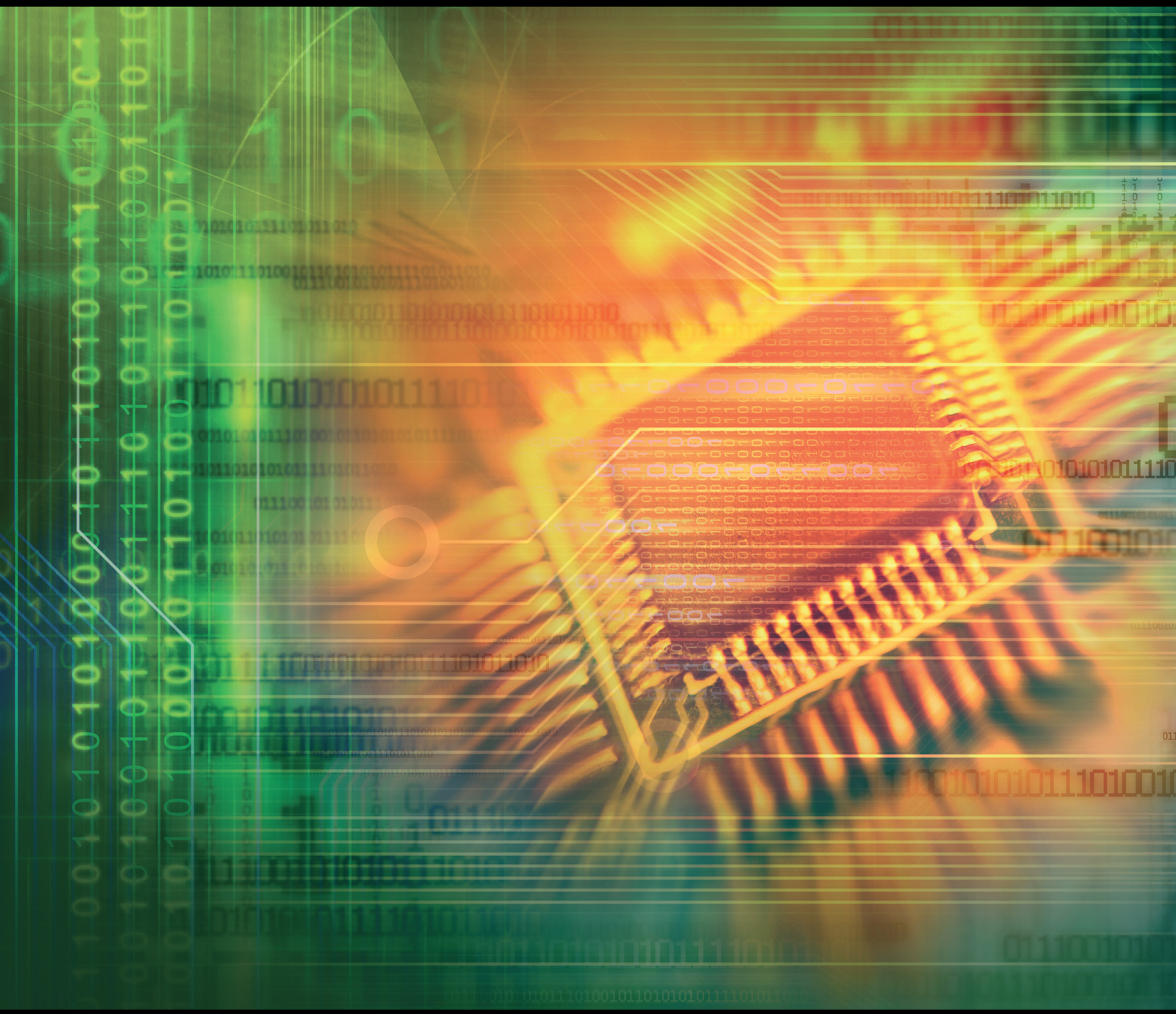

Evolutionary, Neural and Fuzzy Systems for Smart and Micro Grids

Journal of Electrical and Computer Engineering

Evolutionary, Neural and Fuzzy Systems for Smart and Micro Grids

Lead Guest Editor: Alessandro Niccolai
Guest Editors: Mohamed Louzazni and Alfredo Nespoli

Contents

Hindawi
Journal of Electrical and Computer Engineering
Volume 2022, Article ID 5416722, 23 pages
https://doi.org/10.1155/2022/5416722

Research Article

Analysis of Artificial Neural Network: Architecture, Types, and Forecasting Applications

Manogaran Madhiarasan [1] **and Mohamed Louzazni** [2]

[1]*Department of Computer Science and Engineering, Indian Institute of Technology Roorkee, Roorkee, Uttarakhand 247667, India*
[2]*Chouaib Doukkali University of El Jadida, National School of Applied Sciences, Science Engineer Laboratory for Energy, El Jadida, Morocco*

Correspondence should be addressed to Manogaran Madhiarasan; mmadhiarasan89@gmail.com

Received 30 September 2021; Revised 26 October 2021; Accepted 25 March 2022; Published 18 April 2022

Academic Editor: Jit S. Mandeep

The artificial neural network reduces humanity and society's burden to solve complex problems highly efficiently. Artificial neural networks resemble brain activities based on the acquired training samples used for various applications such as classification, regression, prediction, smart grid, natural language processing, image processing, medical diagnosis, and so on. This paper illustrates the different artificial neural network architectures, types, merits, demerits, and applications. Therefore, this paper provides valuable information to students and researchers to enrich their knowledge about an artificial neural network and research it. This paper also proposed a multilayer-perceptron-neural-network-based solar irradiance forecasting model, an improved backpropagation neural network-based rainfall forecasting model, and an Elman neural network-based temperature forecasting model. The performances of the proposed neural network-based forecasting models are analyzed with various hidden neurons and validated using the acquired real-time meteorological data. The proposed neural network forecasting models achieve rigorous results with reduced errors for the considered applications and aid sustainability.

1. Introduction

In the modern world, ANN is actively replacing the existing methods; this motivated us to address the issue of ANN and made interest in the quest of ANN and provided the complete guideline to the reader about the ANN types, architecture, and applications of ANN. The network that resembles or mimics the biological human brain functions to accomplish a given task is an artificial neural network. In a neural network, one neuron to the other neuron connection exists with some strength known as weight or synaptic weight. The on and off state of a neuron is decided by the threshold function. The perceptron concept was introduced in 1958 by Frank Rosenblatt [1], which is the ability to learn with the single-layer network. The limitation is if the data points are not linearly separable, it cannot solve the problem. Still, many research activities are required to address the perceptron network linear separability issue. Inputs usually are binary, bipolar, and the real-time value from the environment. Many forecasting models are attempted in the literature, but simple, feasible, easy to implement, and accurate forecasting is one of the thrust research fields. In neural network-based forecasting, an interpretable machine learning tool is important [2, 3], and feature selection/extraction is a preprocessing method used to extract important relevant input features [4], data-driven, hybrid, ensemble, and deep neural network aid effective solutions [5–10]. Recently, some researchers performed data-driven-based forecasting [11–13]. In forecasting applications, variability is caused because of the measurement shift and noise. The uncertainty about measurement shift and noise can be overcome by proper commissioning, data evaluation, quality check, sensor calibration, and usage of on-site measurement data [9].

1.1. Comparison between the Human Brain and AI (Artificial Intelligence)

(i) The machine system involves step-by-step procedures and instructions, but humans have fewer processing steps because of the massively parallel

operation. In this aspect, humans are ahead of artificial intelligence.

(ii) Regarding the size and complexity aspect, the human biological brain has 10^{11} numbers of neurons approximately and 10^{15} numbers interconnecting with that brain size; this is many neurons. Interconnection is highly impossible based on AI; hence, complexity exists in the human brain both outside of dendrites and inside of cell body computation, but it delays the artificial intelligence process.

(iii) Regarding the strength (or) the synaptic weight of interconnection, information has been stored in the machine having replaceable storage, but the brain has an adaptable storage system.

(iv) The brain has a much high fault tolerance ability compared to a computer and artificial intelligence machine.

(v) Control mechanisms: the retrieval of corrupted information is complicated for the human brain than the machine, so the control mechanism is more difficult for the human brain than the machine.

1.1.1. Motivation. Practical examples: babies or kids can differentiate fruit; guava and green apple both are green in color and shape, but with respect to experience and unique features, the baby or kid determine green apple and guava if we include green mango, and green apple baby can identify similarly ANN-based acquired knowledge about the trained data sets. It has the generalization ability to identify the unknown data sets correctly.

The learning or training process is the stage; the network can acquire knowledge about the situation or environment. The acquired knowledge is stored in the synaptic weights. According to the structural interlinkages of neurons (computational elements), activation function, and weight computation process (learning algorithm), the artificial neural networks can be classified into various types, starting from Mcculloch and Pitts network to present hybrid neural networks.

In a single-layer neural network model, the hidden layer does not appear, so only single connection linkages exist from input to output. A multilayer neural network consists of more than one connection linkage from the input to the output, which can solve challenging and complex problems.

The network does not have feedback, and information can flow from the input layer to the output layer via one or more hidden layers known as a feedforward neural network. Examples of feedforward neural networks are backpropagation, multilayer neural network, radial basis neural network, etc.

The neural network consists of feedback, and information can flow from the input layer to the output layer via one or more hidden layers, and vice versa known as a feedback neural network. Examples of feedback neural networks are the Hopfield network, Elman network, and so on.

1.2. Contribution. This paper has the following contributions:

(i) Give a clear understanding of the comparison between the human brain and artificial intelligence.

(ii) Discuss the development background of an ANN, artificial neural network generalized procedural steps with diagrammatic explanation, typical structure, and applications of artificial neural networks.

(iii) Propose various types of artificial neural networks, like multilayer perceptron neural network, improved backpropagation neural network, and Elman neural network for solar irradiance forecasting, rainfall forecasting, and temperature forecasting, respectively, to aid sustainability.

1.3. Highlights of This Paper

(i) Acquire knowledge of the primary artificial neural network types and applications

(ii) Discuss various ANN architectures, types, and applications

(iii) Propose a solar irradiance forecasting model using MLPNN (Multilayer perceptron neural network)

(iv) Suggest a rainfall forecasting model using IBPNN (Improved Backpropagation Neural Network)

(v) Present a temperature forecasting model using ENN (Elman neural network)

(vi) Carry out various hidden neuron-based analyses

(vii) Propose proved validity of forecasting models in real-time data

(viii) Achieve rigorous forecasting outcomes with reduced errors regarding the proposed forecasting model

(ix) Analyze the different neural network models and familiarize the reader with the forecasting applications

1.4. Development Background of Artificial Neural Network. The motivation of Artificial Neural Network (ANN) is the biological system's parallel and distributed processing. In 1986, McClelland et al. [14] developed an intelligent machine with artificial intelligence, but searching for the solution is the problem with this model. Hence, many heuristic searches address the task accomplishment, and the rule-based approach addresses the representation problem. Table 1 represents the ANN development in the literature for more clarity.

1.4.1. Second Generation Neural Networks. The second generation neural networks are as follows:

(i) Perceptron: for specific learning rules, the network can learn with known target values (supervised learning rule)

Table 1: Development of ANN in the literature.

Year	Authors	Proposed model
1943	Mcculloch and Pitts [15]	Perceptron network with two artificial neurons.
1949	Hebb [16]	Hebbian learning rule.
1958	Rosenblatt [1, 17]	Perceptron network models.
1960	Widrow and Hoff [18]	Adaline neural network.
1962	Widrow [19]	Madaline neural network.
1964	Zadeh [20]	Fuzzy logic.
1982	Hopfield [21]	Hopfield network (recurrent).
1986	Rumelhart et al. [22]	Backpropagation neural network.
1988	Chang and Yang [23]	Cellular neural network (communication exists between only neighboring neurons).
1995	Cortes and Vapnik [24]	Support vector machine.
2002	Gerstner and Kistler [25]	Spiking neural network.
2012	Hinton [26]	Deep learning neural network.

(ii) Backpropagation: based on the various learning methods, the network can learn and adapt the learning data set to known target values (supervised learning rules)

(iii) Kohonen neural network or Self-Organizing Map (SOM): the network learns without knowing the target values (unsupervised learning rule)

(iv) Radial basis neural network (supervised learning rule)

(v) Adaptive resonance theory (unsupervised learning rule)

(vi) Elman neural network (supervised learning rule)

(vii) Hopfield neural network (unsupervised learning rule)

(viii) Special networks (unsupervised and supervised learning rules) like support vector machine

1.4.2. Third Generation Neural Network. Spiking neural network: in this neural network, the limitation of MLP, like cycle firing, has been avoided. This model acquires the firing of biological neurons based on spikes.

1.4.3. Fourth Generation Neural Network. The fourth-generation neural network can be classified into two types as follows:

(i) Deep learning neural network: the deep learning neural network can overcome the gradient vanishing problem over one number of hidden layers

(ii) Hybrid neural network: using both artificial neural network and optimization algorithms, a combination of physical and statistical methods, and so on, makes a hybrid neural network that overcomes the individual network's limitations

2. Generalized Algorithm for Artificial Neural Network

The algorithm in neural networks is nothing but a step-by-step procedure to accomplish a specific task. We showed the generalized algorithm of an artificial neural network in Figure 1, which comprises the following steps as follows:

Step 1. Start the neural network design phase, choose the appropriate neural network model of the artificial neural network (feedforward or feedback, or special neural network, or hybrid model).

Step 2. After selecting a neural network model design, the proposed model includes the number of input parameters, the number of hidden layers, the number of hidden neurons, and so on.

Step 3. After completion of a network design process, initialize the proposed model.

Step 4. After initialization, for the chosen application, collect the data set and perform the data normalization process to eliminate the data discrepancy and missing data and improve the output accuracy. Meanwhile, divide the collected data set into two portions: the training phase and the testing phase.

Step 5. After the data collection and normalization process, learn the proposed neural network with a training data set.

Step 6. Check the proposed neural network's output and whether there is a minimal lead error and verify if the performance is acceptable or not. If the proposed neural network model's performance during the training phase is satisfactory with minimal error, then go for the testing phase. Else, the performance was not up to the mark; then again go to Step 2. The process continues until a match with the set goal.

Step 7. After completing the training phase, perform the proposed neural network model's testing process on the testing data set (the testing data sets are unseen raw data specified during the training phase).

Step 8. After completion of the testing phase, check if the proposed neural network model can achieve generic performance and generalize it well or not. If it generalizes well, record the output of the proposed neural network model; else again perform the remodeling of the neural network to

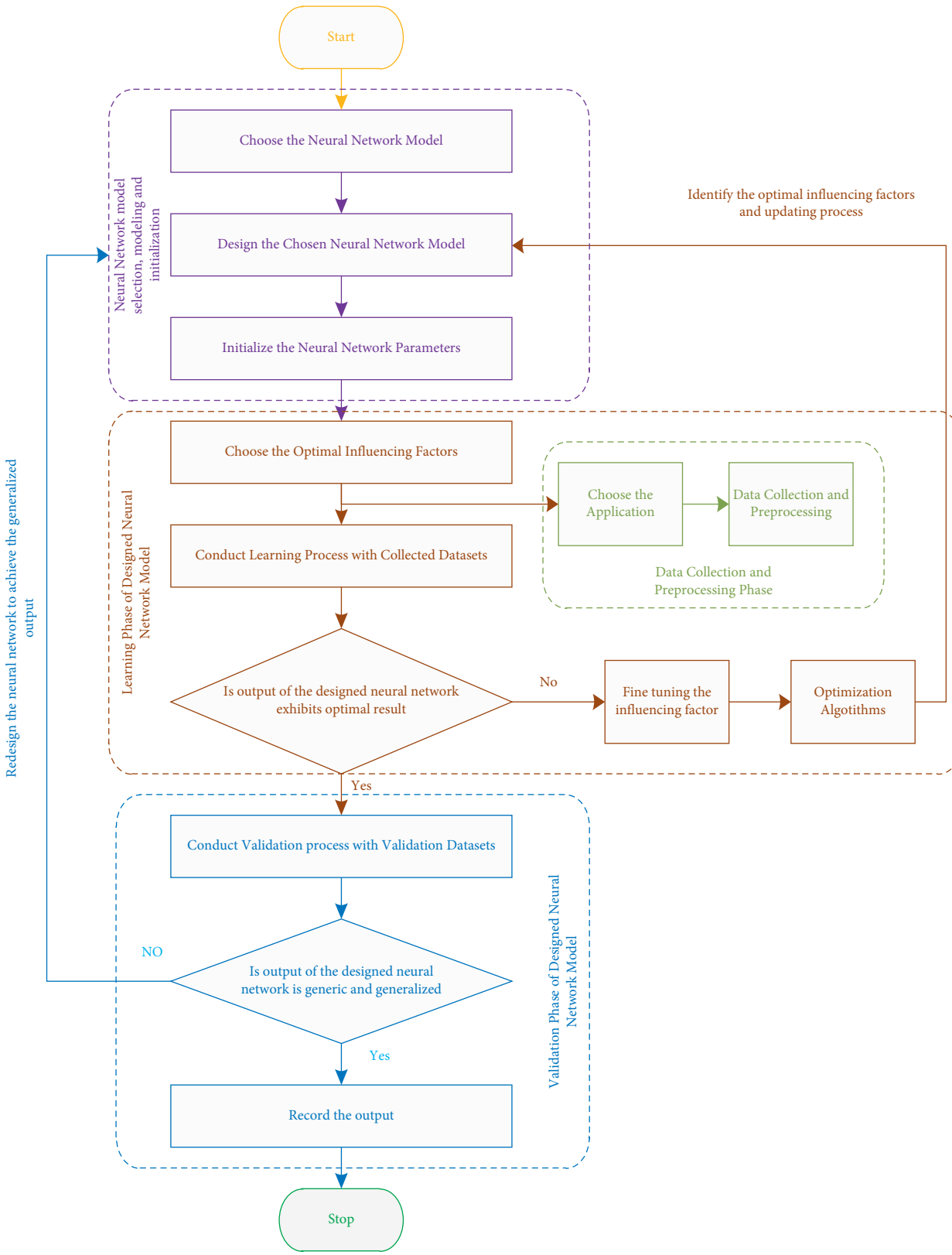

Figure 1: Generalized algorithm of artificial neural network.

achieve the generalized outcome (both training and testing phases lead to an optimal result with minimal error).

Step 9. Stop the process.

3. Applications of Artificial Neural Networks

Artificial neural network applications are not confined to the specific domain; it has a wide variety of applications. An artificial neural network has scope for various applications. Some applications are tabulated in Table 2. The artificial neural network has multiple applications, but not limited content, and it can cover all fields. Hence, it is an interdisciplinary field.

Virtual reality, decision support system (medical science and engineering fields), control engineering, data mining, computer vision, image, pattern recognition, human-machine interface, and few ANN applications. A system that can efficiently and intelligently solve the problem with computation ease is known as an expert system. It poses the ability to learn the environment, think, and apply the gained experience to complete the given task without assistance from the human being.

The system with many acquired knowledge based on many examples, wholly deriving the description of patterns and acquiring knowledge, is a complex problem in pattern recognition, natural language processing, speech, and computer vision applications. The human recalls the pattern, but the machine recall of the data pattern can be in the form of handwriting speech even though the sound of communication is different at various levels in the case of appropriate human identification . The pattern was not clearly defined but also was based on the knowledge humans identified; why not a machine can identify? This question arises from the leading research for the development of existing models in the field of ANN. The human identifies and recognizes the pattern or input based on various samples and examples' continuous learning ability.

In medical practice, ANN is used for medical disease diagnostics because identifying the disease is a challenging task for the medical practitioner and doctor because there will be an overlap of symptoms of various illnesses. Hence, there are no specific guidelines about disease identification based on the medical practice's experience and knowledge; doctors are suggesting the appropriate treatment for the patients. Sometimes, due to human error, patients were affected and they suffered unfair treatment because of the diseases' improper identification. To mitigate the above-said problems, nowadays, an artificial neural network occurs with a vital role in diagnosing patients' conditions.

A game-playing, self-regulated vehicle, self-control expert system, natural language processing, robotics, etc., are some thrust research fields of AI.

Forecasting, regression, classification, and diagnosis of diseases is based on the medical field's symptoms, computer vision, natural language processing (NLP), engineering, and science applications; the artificial neural network is widely used nowadays because of the promising solution to the challenging problem.

4. Proposed Various Artificial Neural Network for Various Forecasting Applications

Although artificial neural networks are suitable for various applications, this paper carries out modeling and analyzes artificial neural networks' effectiveness in forecasting applications like solar irradiance forecasting, rainfall forecasting, and temperature forecasting to aid sustainability. The roadmap of the proposed forecasting model is shown in Figure 2.

4.1. Proposed Multilayer Perceptron Neural Network for Solar Irradiance Forecasting. This paper proposed five meteorological input parameters based on a multilayer perceptron neural network [27]. The multilayer perceptron neural network (MLPNN) consists of one or over one hidden layer, which performs better in computational efficiency than a single-layer perceptron neural network. It belongs to the feedforward neural network and is associated with a supervised learning rule to explore synaptic weight values, and it has a complex problem-solving ability.

The proposed multilayer perceptron neural network is arranged into an input layer, one or more hidden layers, and an output layer. Regarding the hidden layers and nonlinear transfer function, the multilayer perceptron neural network can handle linear and nonlinear relationships between the input and output vectors. In the hidden layer, the hyperbolic tangent sigmoid activation function (nonlinear transfer function) is adopted, and the proposed neural network is trained by employing the backpropagation gradient descent learning rule. The proposed multilayer neural network induces sped-up convergence because it is a fully connected network.

The proposed multilayer perceptron neural network-based forecasting model for solar irradiance forecasting considers the solar irradiance impacting parameters as the inputs such as Solar Irradiance (SI), Temperature (TD), Wind Speed (WS), Dew Point (DP), and Cloud Cover (CC). These five meteorological input parameters are of much impact on solar irradiance. Hence, these parameters are accounted as the input parameters for the proposed neural network. The forecasted solar irradiance is viewed as the output neuron in the single output layer.

The proposed five input-based multilayer perceptron neural networks aim to achieve the best solar irradiance forecast to reduce the minimum error values. The proposed five input-based multilayer perceptron neural networks for solar irradiance structural design are depicted in Figure 3. Table 3 presents the proposed multilayer perceptron neural network design parameters. For the proposed neural network, model-independent computation is performed for each of the layers present in the neural network with respect to the received data. The computed outcomes are transferred to the next immediate layer as an input. Then, the neural network output is then obtained from the output layer; this process flow is clearly understood by Figure 3. During the training process, the involved computations are given as follows.

Table 2: Applications of ANN in various fields.

	Field	Application
ANN (Artificial Neural Network)	Computer science and engineering	NLP (natural language processing) Human machine interface Image processing Virtual reality Data mining Pattern recognition Image and pattern classification
	Electrical and electronics engineering	Fault identification Process and control system Systems integration Forecasting of energy and power
	Civil engineering	Design of optimal structure Material selection and decision making
	Mechanical engineering	Robotics Process optimization Material design
	Aeronautical engineering	Aircraft design Satellite and space application
	Medical science	Classification, identification, and diagnosis of diseases Decision support system
	Environmental engineering	Weather forecasting Rainfall forecasting
	Other fields	Economic forecasting Forex forecasting

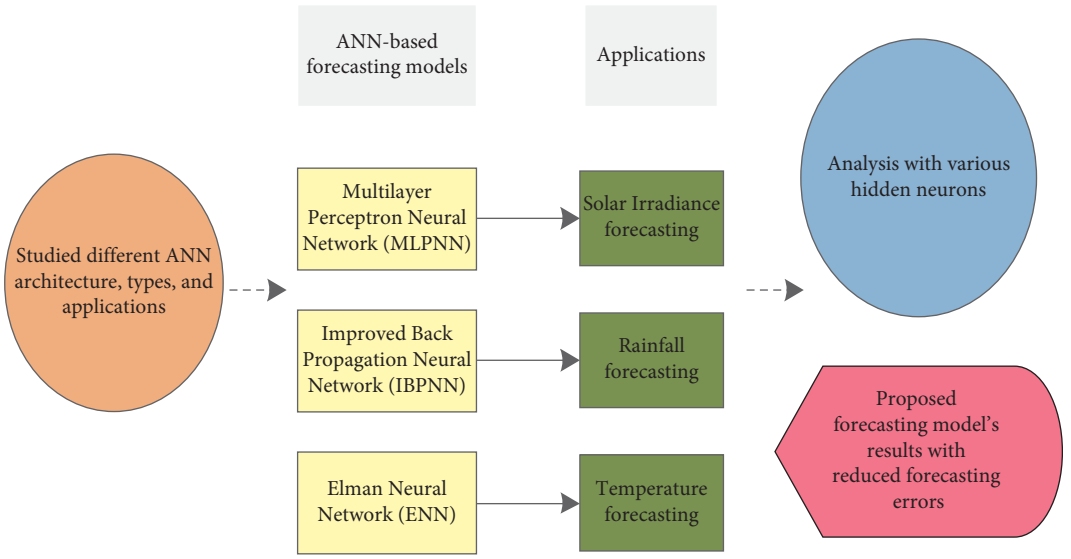

Figure 2: Proposed forecasting model road map.

The proposed MLPNN input vector:

$$K = [SI, TD, WS, DP, CC]. \quad (1)$$

The proposed MLPNN output vector:

$$J = [SI_f]. \quad (2)$$

The proposed MLPNN synaptic weight vectors between the input vector to the hidden vector:

$$SV = \begin{bmatrix} SV_{11}, SV_{12}, \ldots, SV_{1h}, SV_{21}, SV_{22}, \ldots, SV_{2h}, SV_{31}, SV_{32}, \ldots, SV_{3h}, \\ SV_{41}, SV_{42}, \ldots, SV_{4h}, SV_{51}, SV_{52}, \ldots, SV_{5h} \end{bmatrix}. \quad (3)$$

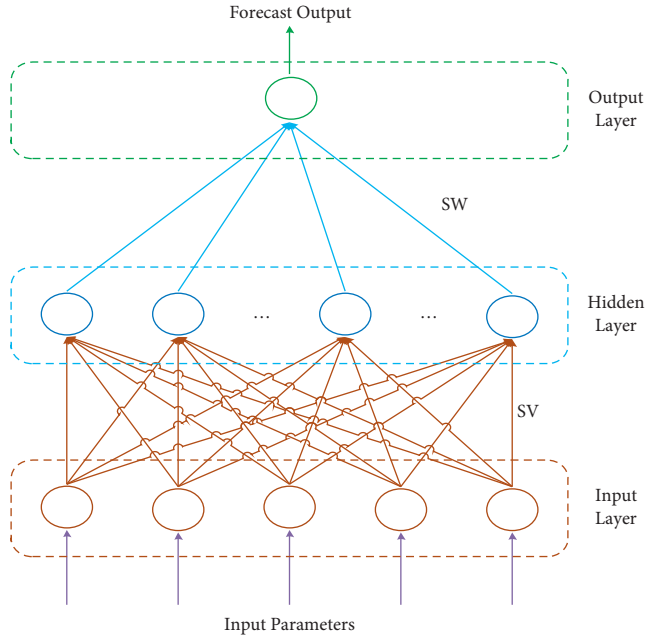

Figure 3: Structural design of the proposed MLPNN.

Table 3: Designed parameters of the proposed various artificial neural networks.

Improved backpropagation neural network	Multilayer perceptron neural network	Elman neural network
Input neuron = 5	Input neuron = 5	Input neuron = 5
Hidden layer = 1	Hidden layer = 1	Hidden layer = 1
Output neuron = 1 RF_f	Output neuron = 1 SI_f	Output neuron = 1 TD_f
Epochs = 2000	Epochs = 2000	Epochs = 2000
Learning rate = 0.01	Learning rate = 0.1	Learning rate = 0.1
Momentum factor = 0.9	Threshold = 1	Threshold = 1
Threshold = 1		

The proposed MLPNN obtains the net input of the hidden layer and subsequently the output of the hidden layer,

$$Y_q = f\left(\sum_{p=1}^{5}\sum_{q=1}^{h} K_p SV_{pq}\right), \tag{4}$$

where K is the input vector, SV is the synaptic weights between the input layer and hidden layer, and h is the number of hidden neurons.

The proposed MLPNN synaptic weight vectors between the hidden to output vector:

$$SW = [SW_1, SW_2, \ldots\ldots, SW_h]. \tag{5}$$

The proposed MLPNN obtains the net input of the output layer and subsequently its neural network final output:

$$Z = f\left(\sum_{q=1}^{h}\left(Y_q SW_q\right)\right), \quad q = 1, 2, \ldots.., h, \tag{6}$$

where SW is the synaptic weight between the hidden layer and output layer, and "f" is the activation function, namely, the tangent sigmoidal activation function.

4.2. Proposed Improved Backpropagation Neural Network for Rainfall Forecasting. The multilayer feedforward neural network with a momentum-based backpropagation learning algorithm is known as the proposed Improved Backpropagation Neural Network (IBPNN) [28]. IBPNN can balance between generalization and the network's memorization. The proposed improved backpropagation neural network is arranged into the input layer, hidden layer, and output layer. The proposed improved backpropagation neural network training stages are classified into three phases: feedforward stage, error computation stage, weight modification, and update stage. The processing elements present in the proposed feedforward neural networks perform an independent computation based on a considered set of input data and synaptic weights with a continuous differential activation function, and the obtained outcomes are passed to the successive layers, and then a final output is achieved from the output layer, which is compared with the target for error computation. Evaluated error is propagated

backward via the output layer-hidden layer-input layer to achieve minimal error.

For the proposed improved backpropagation neural network based on the given set of training inputs and target pairs, the synaptic weights changed and updated, leading to accurate rainfall forecasting with minimal error. The structural design of the proposed five-input-based improved backpropagation neural network for rainfall forecasting is illustrated in Figure 4.

The rainfall is influenced by various variables such as temperature, precipitation of water content, wind speed, and relative humidity. Hence, the proposed neural networks consider these variables as the neural network's inputs to overcome the variance in the atmosphere. The proposed improved backpropagation neural network learning algorithm includes a momentum factor, making the neural network get faster convergence.

$(K_1, K_2, K_3, K_4, K_5: J) =$ (Rainfall, Precipitation of Water Content, Temperature, Relative Humidity, Wind Speed: Forecasted Rainfall).

$$(K_1, K_2, K_3, K_4, K_5: J) = (RF, PWC, TD, RH, WS: RF_f), \tag{7}$$

where RF_f is the forecasted rainfall.

The proposed IBPNN input vector:

$$K = [RF, PWC, T\ D, RH, WS]. \tag{8}$$

The proposed IBPNN output vector:

$$J = [RF_f]. \tag{9}$$

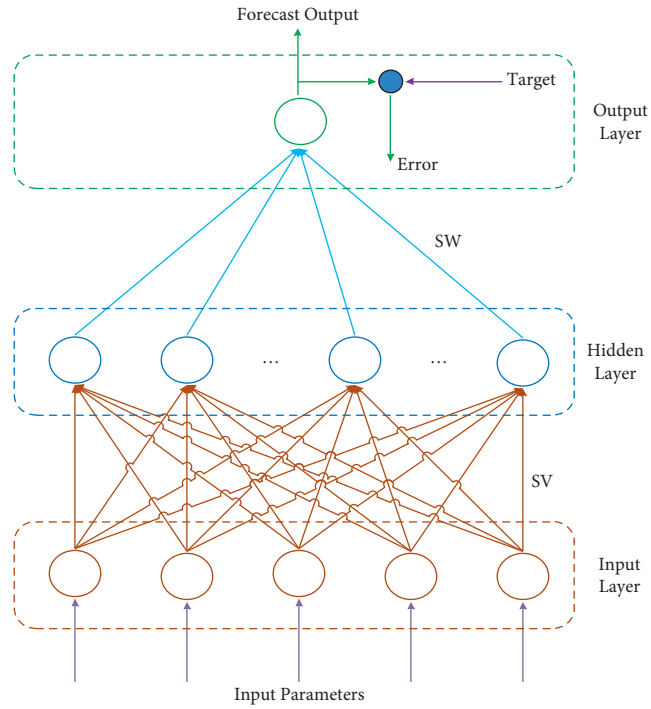

Figure 4: Structural design of IBPNN.

The proposed IBPNN synaptic weight vectors from the input layer to the hidden layer:

$$SV = \begin{bmatrix} SV_{11}, SV_{12}, \ldots, SV_{1h}, SV_{21}, SV_{22}, \ldots, SV_{2h}, SV_{31}, SV_{32}, \ldots, SV_{3h}, \\ SV_{41}, SV_{42}, \ldots, SV_{4h}, SV_{51}, SV_{52}, \ldots, SV_{5h} \end{bmatrix}. \tag{10}$$

The proposed IBPNN net input of the hidden layer:

$$Y_{inq} = \sum_{p=1}^{5} \sum_{q=1}^{h} K_p SV_{pq}. \tag{11}$$

The proposed IBPNN output of the hidden layer:

$$Y_q = f\left(\sum_{p=1}^{5} \sum_{q=1}^{h} K_p SV_{pq} \right). \tag{12}$$

where K is the input of IBPNN, SV is the synaptic weights between the input layer and hidden layer, and h is the number of hidden neurons.

The proposed IBPNN synaptic weight vectors from the hidden layer to the output layer:

$$SW = [SW_1, SW_2, \ldots\ldots, SW_h]. \tag{13}$$

The proposed IBPNN net input of the output layer:

$$Z_{in} = \sum_{q=1}^{h} (Y_q SW_q). \tag{14}$$

The proposed IBPNN output:

$$Z = f\left(\sum_{q=1}^{h} (Y_q SW_q) \right), \quad q = 1, 2, \ldots.., h, \tag{15}$$

where SW is the synaptic weight between the hidden layer and the output layer and f is the activation function.

The proposed IBPNN computed error in the output layer:

$$E = (T_r - Z) f'(Z_{\text{in}}), \tag{16}$$

where $f'(Z_{\text{in}})$ is the derivative of the net input of the output layer.

The evaluated error (E) is propagated back to the hidden layer.

In the proposed IBPNN, each hidden neuron $(Y_q, q = 1, 2, \ldots, h)$ sums its delta inputs from the output layer neurons:

$$E_{\text{in}q} = \sum_{q=1}^{h} ESW_q. \tag{17}$$

The proposed IBPNN error in the hidden layer:

$$E_q = E_{\text{in}q} f'\left(Y_{\text{in}\,q}\right), \tag{18}$$

where $f'(Y_{\text{in}q})$ is the derivative of the net input of the hidden layer.

The computed error (E_q) is propagated back to the input layer to minimize the error during the backpropagation stage:

$$\text{The proposed IBPNN error in the output layer, } = [E]. \tag{19}$$

$$\text{For the proposed IBPNN error in the hidden layer, } = \left[E_j\right]. \tag{20}$$

The proposed improved backpropagation neural network mathematical equations for the synaptic weight updating process were as follows:

$$SW_q(n+1) = SW_q(n) + \alpha EY_q + \eta\left[SW_q(n) - SW_q(n-1)\right], \tag{21}$$

$$SV_{pq}(n+1) = SV_{pq}(n) + \alpha E_q k_p + \eta\left[SV_{pq}(n) - SV_{pq}(n-1)\right], \tag{22}$$

where α is the learning rate and η is the momentum factor.

The synaptic weights are updated and changed using the mathematical equations (21) and (22). The learning stages of the proposed neural network and weight updating process are continued in the proposed IBPNN until attaining the stopping condition (i.e., set value).

4.3. Proposed Elman Neural Network for Temperature Forecasting. The feedback neural network has advantages over the feedforward network; with feedback from the output, the neural network stability and performance can be improved. In a feedback neural network, Elman neural network (ENN) is a famous feedback neural network, which Elman suggested in 1990 [29–31]. Because of the superior performance, Elman network can be used for various applications such as forecasting, speech recognition, modeling, and control. Like the feedforward neural network arranged into the input layer, hidden layer, and output layer, one more layer is also added into the feedback neural network: the feedback layer or recurrent layer. The feedback storage and memory retaining have been done with the help of the recurrent layer. It also copies the one-step delay in the hidden layer. With the help of the internal connection proposed, Elman neural network dynamic characteristics are achieved. The proposed Elman neural network-based forecasting model hidden layer is associated with the hyperbolic tangent sigmoid activation function, and the output layer is associated with the purelin activation function.

The proposed temperature forecasting model is developed using an Elman neural network with five inputs such as Temperature $(T\ D)$, Dew Point (DP), Solar Irradiance (SI), Wind Speed (WS), and Relative Humidity (RH). The proposed Elman neural network complexity is reduced to a single hidden layer with various hidden neurons and one output layer with a single output neuron, i.e., forecast temperature. The proposed Elman neural network's objective is to achieve the accurate forecasting of temperature with reduced convergence time and minimal error. The structural design of the Elman neural network is shown in Figure 5.

During the training process, the involved computations are given as follows:

$(K_1, K_2, K_3, K_4, K_5: J) =$ (Temperature, Dew Point, Solar Irradiance, Wind Speed, Relative Humidity: Forecast Temperature).

$(K_1, K_2, K_3, K_4, K_5: J) = (T\ D, DP, SI, WS, RH: T\ D_f)$, where TD_f is the Forecast Temperature in Degrees.

Let SV_c be the synaptic weights between the context layer and the input layer.

Let SV be the synaptic weights between the input layer and the hidden layer.

Let SV_2 be the synaptic weights between the hidden layer and the recurrent link layer.

Let SW be the synaptic weights between the hidden layer and the output layer.

Let $h(\cdot)$ be the activation function, namely, the hyperbolic tangent sigmoid activation function adopted for the hidden layer.

Let $f(\cdot)$ be the activation function, namely, the purelin activation function which is adopted for the output layer.

Figure 5 infers that the proposed Elman neural network comprising each layer is performing independent computations on receiving data. The obtained output is passed to the next successive layer, and after that, finally, from the output layer, the neural network output is computed. The proposed Elman neural network has the ability that previous input influences the current input responses. The input $K(X-1)$ passes through the hidden layer that multiplies the synaptic weight (SV) with the association of the hyperbolic tangent sigmoid activation function. In addition to the previous state output $SV_cK_c(X)$, the current input $SVK(X-1)$ was also added, which aids the proposed feedback neural network to efficiently learn the function. The value $K(X)$ is passed through an output layer multiplied by the synaptic weight SW with the association of the purelin activation function.

The proposed ENN input vector:

$$K = [TD, DP, SI, WS, RH]. \tag{23}$$

The proposed ENN output vector:

$$J = \left[TD_f\right]. \tag{24}$$

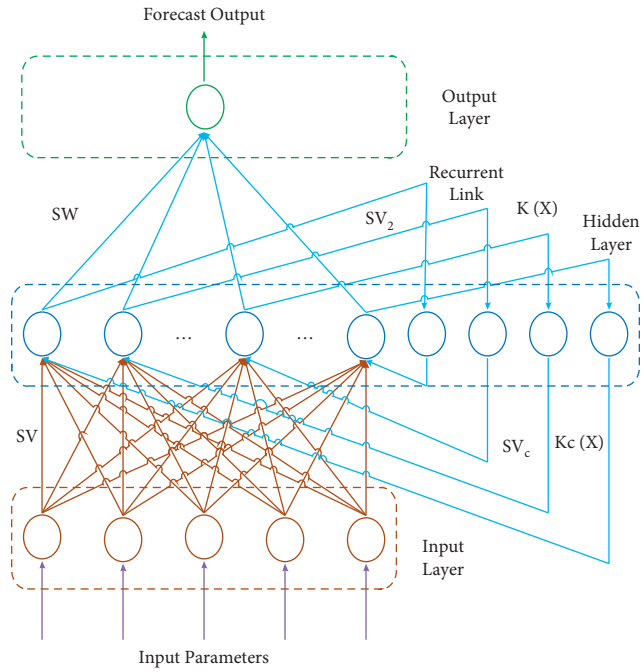

Figure 5: Structural design of ENN.

The proposed ENN synaptic weight vector between inputs to the hidden vector:

$$SV = \begin{bmatrix} SV_{11}, SV_{12}, \ldots, SV_{1h}, SV_{21}, SV_{22}, \ldots, SV_{2h}, SV_{31}, SV_{32}, \ldots, SV_{3h}, \\ SV_{41}, SV_{42}, \ldots, SV_{4h}, SV_{51}, SV_{52}. \ldots, SV_{5h} \end{bmatrix}. \tag{25}$$

The proposed ENN synaptic weight vector of the recurrent link layer vector:

$$SV_2 = [SV_{21}, SV_{22}, \ldots., SV_{2h}]. \tag{26}$$

The proposed ENN synaptic weight vector of the output layer vector:

$$SW = [SW_{11}, SW_{21}, \ldots., SW_{ho}]. \tag{27}$$

The proposed ENN Synaptic weight vector of the recurrent link layer with the input vector:

$$SV_c = \begin{bmatrix} SV_{c11}, SV_{c12}, \ldots, SV_{c1h}, SV_{c21}, SV_{c22}, \ldots, SV_{c2h}, SV_{c31}, SV_{c32}, \ldots, \\ SV_{c3h}, SV_{c41}, SV_{c42}, \ldots, SV_{c4h}, SV_{c51}, SV_{c52}, \ldots, SV_{c5h} \end{bmatrix}. \tag{28}$$

The proposed ENN input:

$$K(X) = h\left(SV_c K_c(X) + SVK(X-1)\right). \tag{29}$$

The proposed ENN output:

$$J(X) = f(SWK(X)). \tag{30}$$

The proposed ENN input of the recurrent link layer:

$$K_c(X) = K(X-1). \tag{31}$$

4.4. Proposed Artificial Neural Network Experimental Implementation. In the current year, forecasting is a vital tool because people can plan according to it. Solar irradiance forecasting is a crucial factor in the solar energy system. Based on the forecasted solar irradiance, solar energy can be estimated to operate better than the power system and the possibility of extracting maximum solar power. It carried out many research works in solar irradiance forecasting [32–34]. Although a more accurate solar irradiance forecasting model is still needed, it motivates the authors to develop multilayer perceptron neural network-based

solar irradiance forecasting. The meteorological center tries to forecast the precise prediction of weather reports (Temperature) and rainfall. The predicted output does not match the current values because these values are highly influenced by the atmosphere variables like wind speed, cloud cover, precipitation of water content, etc. Some researchers endeavor to forecast the rainfall [35–37] and temperature [38–40] because of the volatile nature outperforming the generic forecasting model required. This fact motivates the development of the high accurate forecasting model for rainfall and temperature forecasting based on the proposed feedforward neural network (i.e., improved backpropagation neural network) and feedback neural network (i.e., Elman neural network), respectively.

The design and development stage, training stage, and testing stage are the three stages of the proposed artificial neural networks. The input-related data for the chosen applications are gathered, normalized into the range of zero to one through min-max normalization (variance eliminated), and then the training and testing process of the designed neural network is carried out with the acquired training and testing data sets, respectively. The validity of the proposed neural network-based forecasting model has been proven and analyzed based on the computed error validation process. It requires the proper design in neural network modeling because the improper selection of design parameters leads to poor performance.

4.4.1. Data Collection. For the considered solar irradiance forecasting applications, rainfall forecasting and temperature-related real-time input parameters are acquired from the National Oceanic and Atmospheric Administration, United States.

For the considered solar irradiance forecasting, the related inputs (Solar Irradiance (SI), Temperature (TD), Wind Speed (WS), Dew Point (DP), and Cloud Cover (CC)) data samples are acquired from the period of January 2014 to December 2019, which comprise 175200 total number of data samples of each input.

For the considered rainfall forecasting, the related inputs (Rainfall (RF), Precipitation of Water Content (PCW), Temperature ($T\ D$), Relative Humidity (RH), and Wind Speed (WS)) are acquired from the period of April 2014 to April 2019, which consist of 52560 data samples of each input.

For the considered temperature forecasting application, the related input parameters (Temperature (TD) , Dew Point (DP), Solar Irradiance (SI), Wind Speed (WS), and Relative Humidity (RH)) are acquired from the period of March 2012 to April 2019, which consists of 1051200 data samples of each considered input.

4.4.2. Data Normalization. The data normalization is required because the data collected from the resource center are real-time data that possess the variance with respect to various ranges and various units to remove the variance of the acquired real-time data. The data normalization process, collecting data irrespective of multiple ranges and different units, classifies the data in the range from 0 to 1. In data normalization, various methods are available for this proposed work; min-max normalization adopts the proposed artificial neural network-based forecasting model. The proposed artificial neural network's numerical computation and accuracy can be improved by employing data normalization. The following transformational mathematical equation is used for the normalization of the real-time collected data.

$$\text{Normalized input, } K_p' = \left(\frac{K_p - K_{\min}}{K_{\max} - K_{\min}}\right)\left(K_{\max}' - K_{\min}'\right) + K_{\min}', \tag{32}$$

where K_p is the collected real-time input data, $K_{\min}$ is the minimal input data, $K_{\max}$ is the maximum input data, $K_{\min}'$ is the minimal target value, and $K_{\max}'$ is the maximum target value.

4.4.3. Proposed Artificial Neural Network Modeling. The designed parameters of the proposed artificial neural networks are presented in Table 3. The proposed various artificial neural networks modeling parameter dimensions such as the number of input neurons, hidden neurons, output neurons, the number of epochs, learning rate, momentum factor, and the threshold value are tabulated in Table 3.

The implemented multilayer-perceptron-neural-network- (MLPNN-) based solar irradiance forecasting model inputs are passed to the hidden layer that is multiplied by synaptic weight (SV) with hyperbolic tangent sigmoid activation function. The hidden layer's output is passed to the output layer that is multiplied by synaptic weight (SW) with the purelin activation function. We use the Levenberg-Marquardt training algorithm for the proposed MLPNN-based solar irradiance forecasting model training process.

The proposed improved-back-propagation-neural-network- (IBPNN-) based rainfall forecasting model inputs are transmitted to the hidden layer multiplied by the synaptic weight (SV) utilizing a hyperbolic tangent sigmoid activation function. The hidden layer's output is transmitted to the output layer multiplied by the synaptic weight (SW) with the tangential sigmoid activation function. The training algorithm used for IBPNN is Levenberg- Marquardt back-propagation training algorithm. The momentum factor is included in the learning algorithm, which leads to speed-up convergence.

The designed Elman-neural-network- (ENN-) based temperature forecasting model and the synaptic input weights (SV) are interconnected to the hidden layer using the hyperbolic tangent sigmoid activation function. The hidden layer's output is interconnected to the output layer with synaptic weight (SW) using the purelin activation function. As a result of training, the previous inputs get reflected in the Elman neural network. The training algorithm used for the proposed Elman neural network is

gradient descent with momentum and an adaptive linear backpropagation training algorithm.

For all proposed artificial-neural-network-based forecasting models, training and testing are done through the normalized data set. The validation process is continued until the stopping condition is reached.

4.4.4. Selection of Number of Hidden Neurons in the Proposed Artificial Neural Networks. The most challenging process in the artificial neural network is selecting the required number of hidden neurons to place in the artificial neural network [41–45]. There is no generalized formulation and criterion available for selecting hidden neurons in an artificial neural network. The random selection and trial-and-error methods also take much more time. If the hidden neurons are too low and too high, both condition neural networks do not achieve optimal results. Hence, the proposed artificial neural network, namely, multilayer neural network, improved backpropagation neural network, and Elman neural network with a single hidden layer, is preferred because the neural network with a single hidden layer can solve the problem with less computational difficulty. In that single hidden layer, the hidden neurons are varied from one (1) to fifteen (15). The designed neural network is validated for each considered hidden neuron, and the obtained results are tabulated. According to Tables 4–6, appropriated numbers of hidden neurons are identified for the proposed artificial neural network based on the minimal error and minimal convergence time.

4.4.5. Training and Testing of the Proposed Artificial Neural Network Performance. The proposed solar irradiance forecasting model is built using the training data set. The proposed MLPNN-based solar forecasting model performance is verified based on the testing data set. The acquired data are classified into two sets, like training and testing. The training set comprises 70 percentages of the obtained data samples, and the testing set comprises the remaining unseen 30 percentages of acquired data samples. For the solar irradiance forecasting, the acquired data samples are 175200 real-time data samples, 70% data samples (122640) are used for the training stage, and the unseen data samples (52560) are used for the testing stage of the proposed neural network.

The proposed rainfall forecasting model is built on the training data set, and the proposed IBPNN based rainfall forecasting model performance is verified based on the testing data set. The acquired data are classified into two sets, training and testing, respectively. The training set comprises 70 percentages of the obtained data samples, and the testing set consists of the remaining unseen 30 percentages of obtained data samples. For rainfall forecasting, the acquired data samples are 52560 real-time data samples, 70% data samples (36792) are used for the training stage, and the unseen data samples (15768) are used for the proposed testing stage neural network.

The proposed temperature forecasting model is built on the training data set, and the proposed ENN-based temperature forecasting model performance is verified based on the testing data set. The acquired data are classified into two sets, like training and testing. The training set consists of 70 percentages of the obtained data samples, and the testing set consists of the remaining unseen 30 percentages of acquired data samples. For temperature forecasting, the acquired data samples are 1051200 real-time data samples, 70% of data samples (735840) are used for the training, and 30% of the unseen data samples (315360) are used for the testing stage of the proposed neural network.

The proposed artificial neural network performance is validated based on the training and testing set. The error qualifiers like R, MAPE, MSE, MAE, RMSE, MRE, and Time are used to verify the proposed artificial neural network performance. The number of hidden neurons that leads to reduced error is fixed as the optimal number of hidden neurons in the proposed artificial neural network.

4.4.6. Error Qualifier of the Proposed Artificial Neural Networks. The performance of the proposed various artificial neural networks such as multilayer perceptron neural network, improved backpropagation neural network, and Elman neural network is verified by the evaluated error qualifiers, namely, Correlation Coefficient (R), Mean Absolute Percentage Error (MAPE), Mean Square Error (MSE), Mean Absolute Error (MAE), Root Mean Square Error (RMSE), Mean Relative Error (MRE), and Time in Minutes. The proposed artificial neural network effectiveness is evaluated based on the error qualifiers equations (33)–(38). The following mathematical equations are used for the error computation:

$$MAPE = \frac{100}{N}\sum_{p=1}^{N}\left|\frac{\left(K_p' - K_p^f\right)}{\overline{K}_p}\right|, \tag{33}$$

$$MSE = \frac{1}{N}\sum_{p=1}^{N}\left(K_p' - K_p^f\right)^2, \tag{34}$$

$$MAE = \frac{1}{N}\sum_{p=1}^{N}\left(\left|K_p' - K_p^f\right|\right), \tag{35}$$

$$RMSE = \sqrt{\left(\frac{1}{N}\sum_{p=1}^{N}\left(K_p' - K_p^f\right)^2\right)}, \tag{36}$$

$$\mathrm{MRE} = \frac{1}{N}\sum_{p=1}^{N}\left|\frac{\left(K_p' - K_p^f\right)}{\overline{K}_p}\right|, \tag{37}$$

$$\mathrm{R} = 1 - \left(\frac{\sum_{p=1}^{N}\left(K_p' - K_p^f\right)}{\sum_{p=1}^{N} K_p^f}\right)^2. \tag{38}$$

where N is total number of data samples, K_p' is target output, $\overline{K}_p$is average target output, and $K_p^f$is forecasted output.

Table 4: The proposed five input-based multilayer perceptron neural network statistical performance analyses with various hidden neurons for solar irradiance forecasting.

Number of hidden neurons	Error qualifier						
	R	MAPE	MSE	MAE	RMSE	MRE	Time (min)
1	1	0.0029	7.1344*e*-05	0.0063	0.0084	2.9047*e*-05	3.17
2	1	0.0014	1.8264*e*-05	0.0031	0.0043	1.4451*e*-05	4.13
3	1	8.2990*e*-04	7.3104*e*-06	0.0018	0.0027	8.2990*e*-06	2.03
4	1	0.0020	4.3011*e*-05	0.0043	0.0066	1.9727*e*-05	2.32
5	1	7.2196*e*-04	5.7284*e*-06	0.0016	0.0024	7.2196*e*-06	3.32
6	1	0.0025	7.1011*e*-05	0.0055	0.0084	2.5175*e*-05	1.31
7	1	0.0026	7.4721*e*-05	0.0055	0.0086	2.5515*e*-05	2.03
8	1	8.2778*e*-04	7.9809*e*-06	0.0018	0.0028	8.2778*e*-06	1.48
9	1	7.3968*e*-04	6.2360*e*-06	0.0016	0.0025	7.3968*e*-06	3.32
10	1	7.5442*e*-04	6.5662*e*-06	0.0016	0.0026	7.5442*e*-06	3.50
11	1	0.0018	3.8319*e*-05	0.0040	0.0062	1.8279*e*-05	2.11
12	1	5.1926*e*-04	3.0656*e*-06	0.0011	0.0018	5.1926*e*-06	2.17
13	1	3.2149*e*-04	1.1717*e*-06	6.9914*e*-04	0.0011	3.2149*e*-06	5.04
14	1	**2.3034*e*-04**	**5.9791e-07**	**5.0093e-04**	**7.7324e-04**	**2.3034e-06**	**1.32**
15	1	0.0012	1.7649*e*-05	0.0027	0.0042	1.2348*e*-05	3.02

Bold implies the best results.

Table 5: The proposed five inputs based on improved backpropagation neural network statistical performance analysis with various hidden neurons for rainfall forecasting.

Number of hidden neurons	Error qualifier						
	R	MAPE	MSE	MAE	RMSE	MRE	Time (min)
1	0.98949	8.9725	657.7246	18.1105	25.6461	0.0897	1.21
2	0.1638	100	7.4967*e*+04	201.8431	273.8012	1.000	0.01
3	0.99991	0.7373	5.4600	1.4882	2.3367	0.0074	0.57
4	1	0.2696	0.6398	0.5441	0.7999	0.0027	1.59
5	1	0.0945	0.0864	0.1906	0.2939	9.4451*e*-04	4.15
6	1	0.0344	0.0143	0.0695	0.1194	3.4418*e*-04	1.54
7	**1**	**0.0158**	**0.0042**	**0.0320**	**0.0645**	**1.5841*e*-04**	**1.24**
8	1	0.0203	0.0077	0.0409	0.0880	2.0264*e*-04	1.36
9	1	0.0199	0.0079	0.0401	0.0869	1.9879*e*-04	1.49
10	1	0.0170	0.0066	0.0344	0.0815	1.7022*e*-04	1.52
11	1	0.0357	0.1512	0.0721	0.3889	3.5704*e*-04	1.13
12	1	0.0283	0.0842	0.0572	0.2902	2.8320*e*-04	3.47
13	1	0.0231	0.2452	0.0466	0.4956	2.3092*e*-04	3.10
14	1	0.0191	0.3369	0.0385	0.5804	1.9076*e*-04	5.40
15	1	0.0255	0.6127	0.0515	0.7828	2.5517*e*-04	8.31

Bold implies the best results.

4.5. Validation Experimental Results of the Proposed Artificial Neural Network for Various Forecasting Applications. The proposed artificial-neural-networks-based forecasting models are experimentally simulated in MATLAB platform version 2013 running on Acer computers with Pentium (*R*) Dual-Core processor running at 2.30 GHz with 2 GB of RAM.

4.5.1. Experimental Results of the Proposed Multilayer-Perceptron-Neural-Network-Based Solar Irradiance Forecasting. The designed multilayer-perceptron-neural-network-based solar irradiance forecasting model performance is validated experimentally, and the got results with various numbers of hidden neurons (1–15) are tabulated in Table 4 and analyzed. From the analysis of Table 4, it is observed that the proposed multilayer-perceptron-neural-network-based solar irradiance forecasting model performs better for various hidden neurons.

The proposed forecasting model output is changed drastically by varying the hidden neuron in the proposed multilayer perceptron neural network's hidden layer. The hidden neuron in the hidden layer increases further and makes the neural network unstable, while decreasing the hidden neuron further also leads the neural network to become unstable. Based on the achieved solar irradiance forecasting results among 1 to 15 hidden neurons, the proposed multilayer perceptron neural network contains a single hidden layer that possesses 14 hidden neurons that provide the best outputs with minimal error and reduced convergence time.

Therefore, the proposed multilayer perceptron neural network with five inputs, a single hidden layer, 14 hidden neurons in the hidden layer, and a single output neuron

Table 6: The proposed five input-based Elman neural network statistical performance analyses with various hidden neurons for temperature forecasting.

Number of hidden neurons	Error qualifier					
	MAPE	MSE	MAE	RMSE	MRE	Time (sec)
1	0.6612	0.1299	0.1488	0.3605	0.0066	22
2	1.2701	0.4218	0.2859	0.6494	0.0127	31
3	0.8163	0.1949	0.1837	0.4415	0.0082	29
4	0.6202	0.0684	0.1396	0.2615	0.0062	33
5	1.0752	0.3555	0.2420	0.5962	0.0108	34
6	0.4970	0.0821	0.1119	0.2866	0.0050	33
7	0.1069	0.0035	0.0241	0.0590	0.0011	44
8	0.1013	0.0015	0.0228	0.0384	0.0010	35
9	0.4501	0.0671	0.1013	0.2591	0.0045	42
10	0.9629	0.2676	0.2167	0.5173	0.0096	45
11	**0.1023**	**0.0011**	**0.0230**	**0.0332**	**0.0010**	**22**
12	0.3122	0.0319	0.0703	0.1787	0.0031	46
13	0.1715	0.0025	0.0386	0.0502	0.0017	39
14	0.4440	0.0473	0.0999	0.2175	0.0044	49
15	0.8641	0.2005	0.1945	0.4478	0.0086	51

Bold implies the best results.

structure is identified as the best framework. The obtained output plots based on this structural framework-associated forecasting model are shown in Figure 6. The number of data vs. solar irradiance is presented in Figure 7. The real-time target solar irradiance compared with forecasted solar irradiance is illustrated in Figure 8. Error vs. number of data is shown in Figure 9. Relationship between forecast solar irradiance and real-time target solar irradiance, respectively. Because of the space limitation, portions of the obtained results are shown in Figures 6–9. The 14 hidden neuron-based developed neural network (MLPNN) models forecasting solar irradiance are much matched with the real-time target solar irradiance. Hence, the error values are reduced to the minimal, clearly understood from Figures 7 and 8, respectively.

Figure 8 shows that the proposed neural network with 14 hidden neurons results in a minimal error on the considered data samples. The relationship between forecasted solar irradiance and real-time target solar irradiance is a linear relationship that illustrates that the forecasted solar irradiance accurately matches the real-time target. Hence, the proposed neural network (MLPNN) proved its validity, which is noticed in Figure 9.

4.5.2. Experimental Results of Proposed Improved Backpropagation Neural Network-Based Rainfall Forecasting. The proposed improved backpropagation neural network-based rainfall forecasting model performance is validated experimentally using the collected data, and the obtained results of the proposed neural network with various numbers of hidden neurons (1–15) are tabulated in Table 5. According to the obtained results in Table 5, it is noticed by careful analyses that the proposed rainfall forecasting model based on the improved backpropagation neural network performs very poorly for the hidden neurons 1 and 2 except that for the remaining hidden neurons results in the good output. The IBPNN-based forecasting model achieved outcome is changed drastically with the hidden neurons changes in the proposed improved backpropagation neural network's hidden layer.

In a neural network, the neural network stability and performance are highly affected by hidden neurons. Based on the analysis of the obtained results, it is observed that the proposed improved backpropagation neural network with a single hidden layer and seven hidden neurons in the hidden-layer-based design neural network (IBPNN) achieves superior performance in terms of reduced error and reduced convergence speed compared among other hidden neurons based on design neural networks.

Therefore, the proposed improved backpropagation neural network with five inputs, a single hidden layer, seven hidden neurons in the hidden layer, and a single output layer with one output neuron has been identified as the optimal structural framework of the proposed neural network. The obtained rainfall forecasting plots with seven hidden neurons-based design IBPNN are depicted in Figure 10. Rainfall in mm vs. data samples is shown in Figure 11. Original target rainfall compared with forecast rainfall is illustrated in Figure 12. Evaluation error metric vs. the number of data samples is presented in Figure 13, the relationship between forecast rainfall and original target rainfall, respectively. Because of the space limitation, portions of the obtained results are shown in Figures 10–13.

The considered data sample for the validation of the neural network is represented in Figure 10. In the seven-hidden-neurons-based developed backpropagation neural network model, where the forecast rainfall is a relative value compared with the original target rainfall, the forecasting accuracy is better which is understood from Figure 11. It is observed that the designed IBPNN achieves minimal errors for more clarity; the evaluation error with respect to the data samples is depicted in Figure 12. The relationship between forecast rainfall and original target rainfall is a linear relationship, which illustrates that the forecast rainfall is higher, accurately matched with the original target, which is clearly observed in Figure 13.

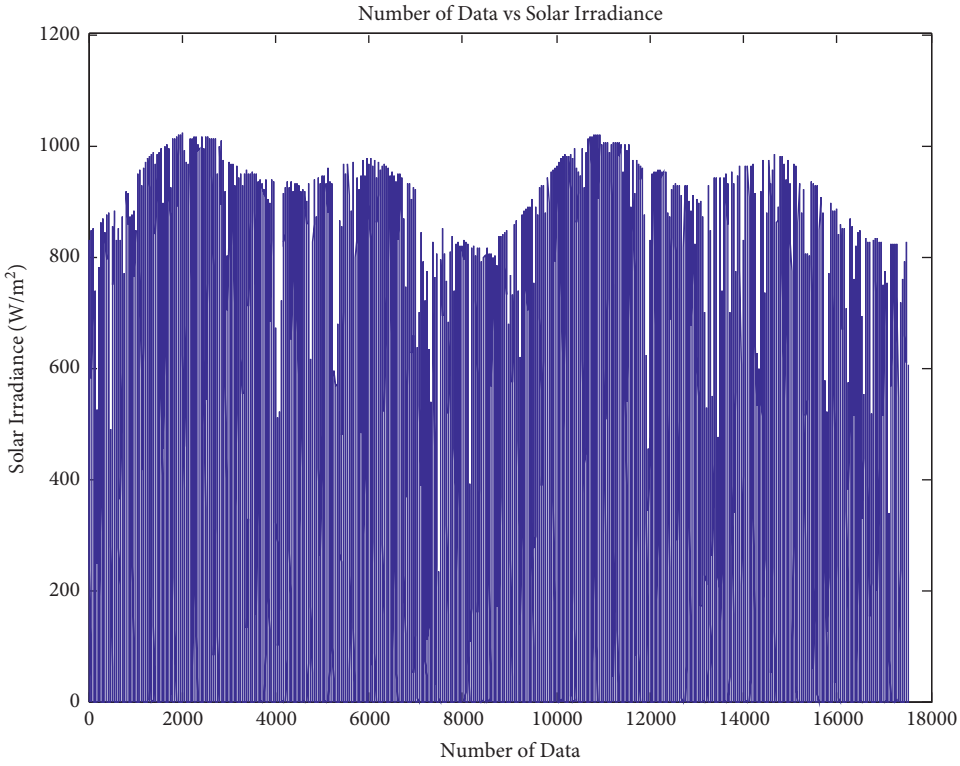

Figure 6: Number of data vs. solar irradiance.

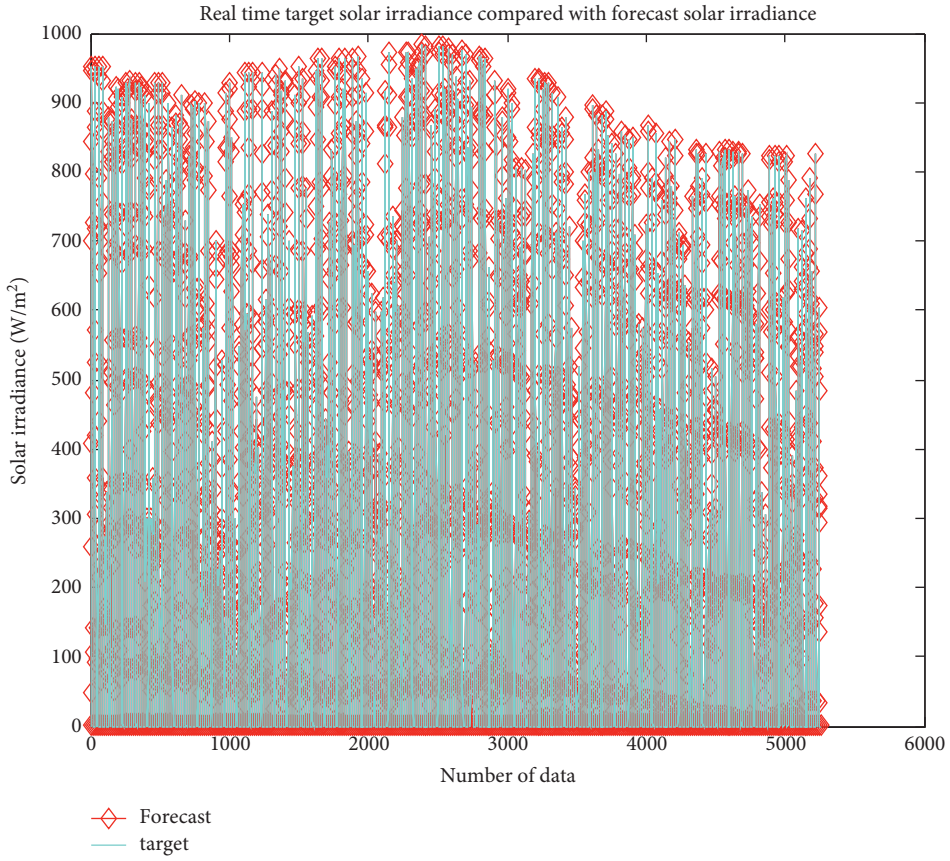

Figure 7: Real-time target solar irradiance compared with forecasted solar irradiance.

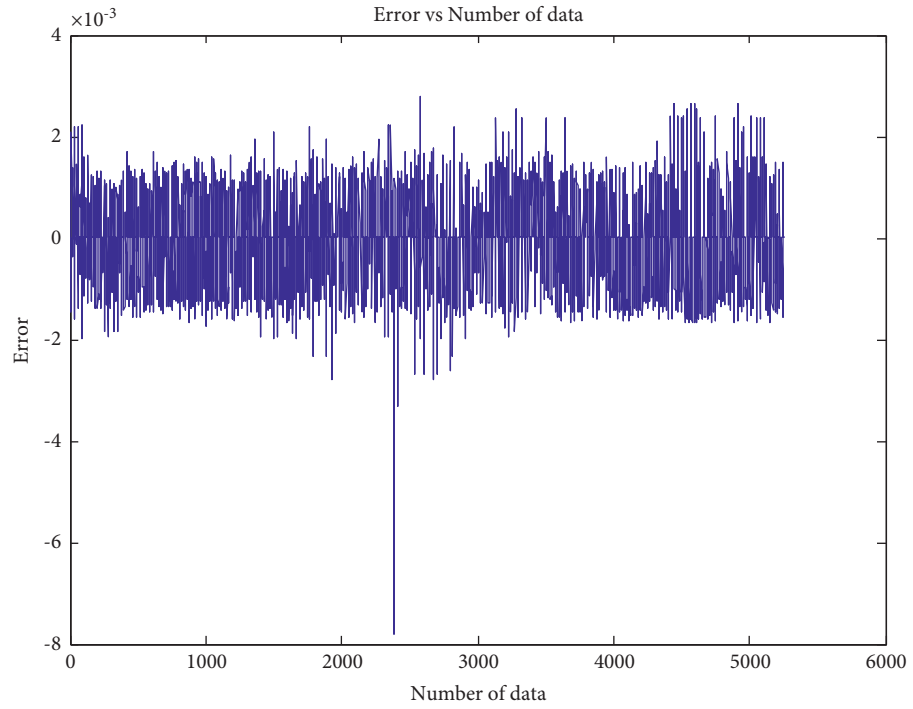

Figure 8: Error vs. the number of data.

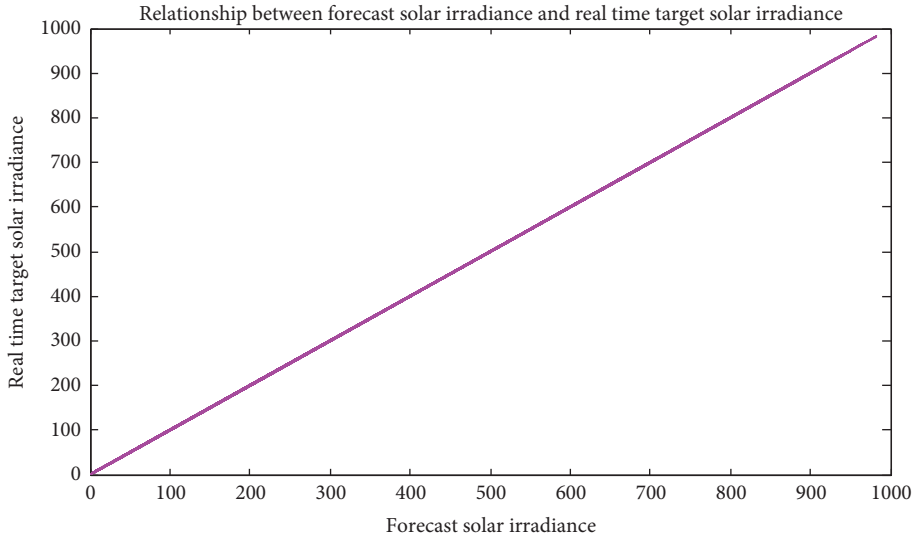

Figure 9: Relationship between forecast solar irradiance and real-time target solar irradiance.

4.5.3. Experimental Results of the Proposed Elman-Neural-Network-Based Temperature Forecasting. The proposed temperature forecasting models based on Elman neural network validated with the acquired data samples and achieved experimental outputs based on different numbers of hidden neurons from 1 to 15 are tabulated in Table 6. According to the achieved results in Table 6, it is observed that the proposed Elman-neural-network-based forecasting model performs well for all hidden neurons. The proposed Elman-neural-network- (ENN-) based temperature forecasting model output is changed drastically due to the number of hidden neurons varying in the proposed Elman neural network's hidden layer.

In a feedback neural network, hidden neurons profoundly influence the aspects of neural network stability and performance convergence. From the result analysis of the obtained outputs, it is noticed that the designed Elman neural network with a single hidden layer and 11 hidden neurons in the hidden layer achieves better performance in terms of reduced error and reduced convergence speed compared among other numbers of hidden neurons based on the designed neural networks. Therefore, the proposed

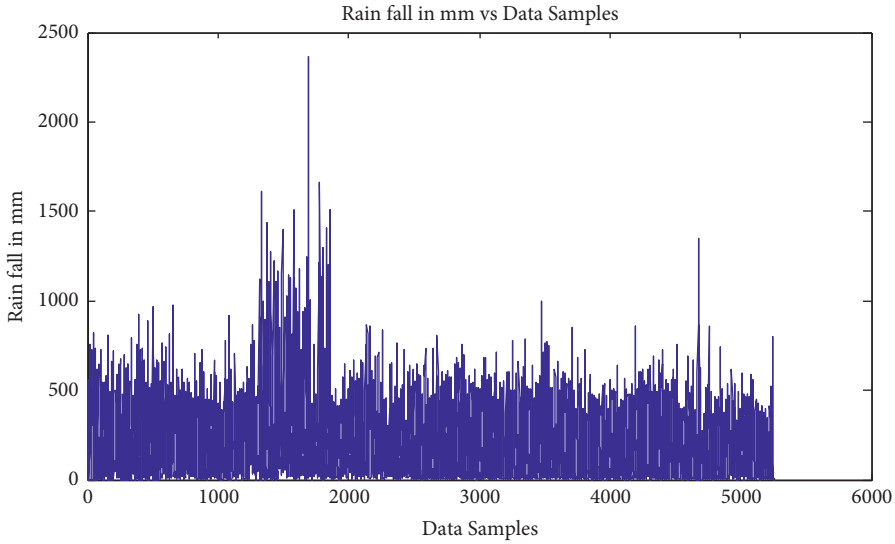

Figure 10: Rainfall in mm vs. data samples.

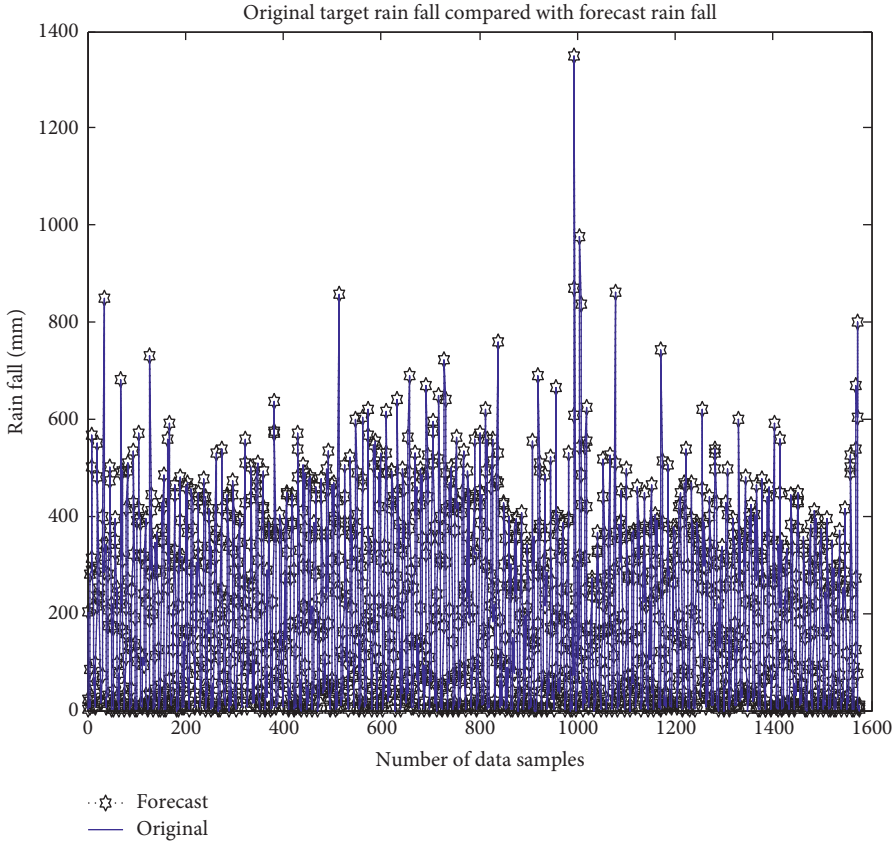

Figure 11: Original target rainfall compared with forecast rainfall.

temperature forecasting model based on Elman neural network with five inputs, a single hidden layer, 11 hidden neurons in the hidden layer, and a single output layer with one output neuron has been identified as the useful structural framework of the proposed neural network.

The obtained temperature forecasting plots with respect to the 11 hidden neuron-based design ENNs are shown in Figure 14. Temperature vs. data samples is presented in Figure 15. Comparison between target and forecasted temperature is presented in Figure 16. Error vs. number of data is shown in Figure 17, the relationship between target and forecast temperature, respectively. Due to the space limitation, portions of the obtained results are shown in Figures 14–17.

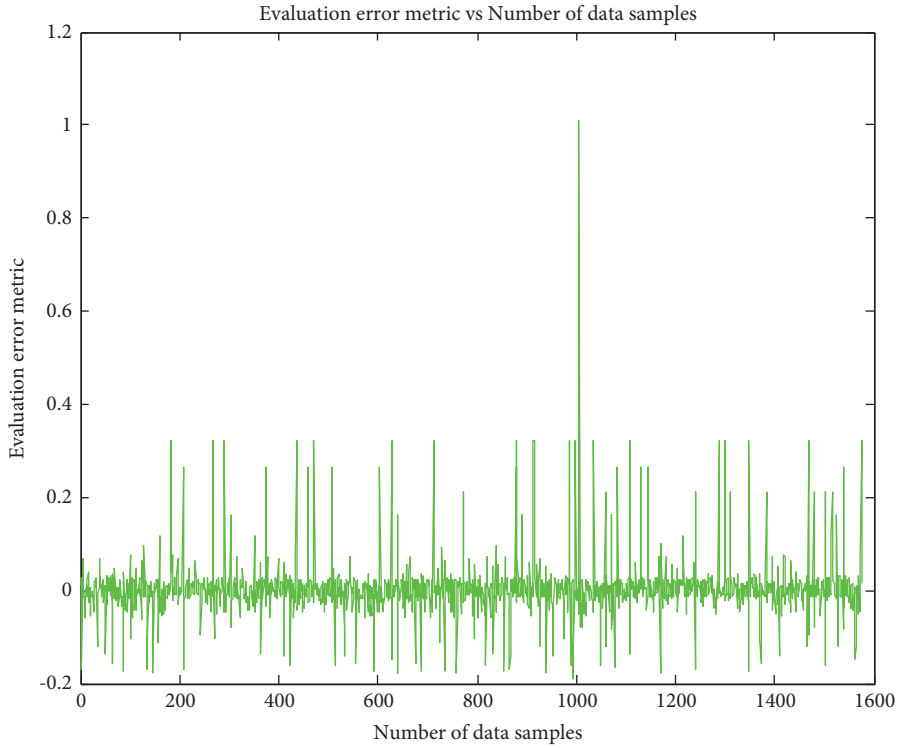

Figure 12: Evaluation error metric vs. the number of data samples.

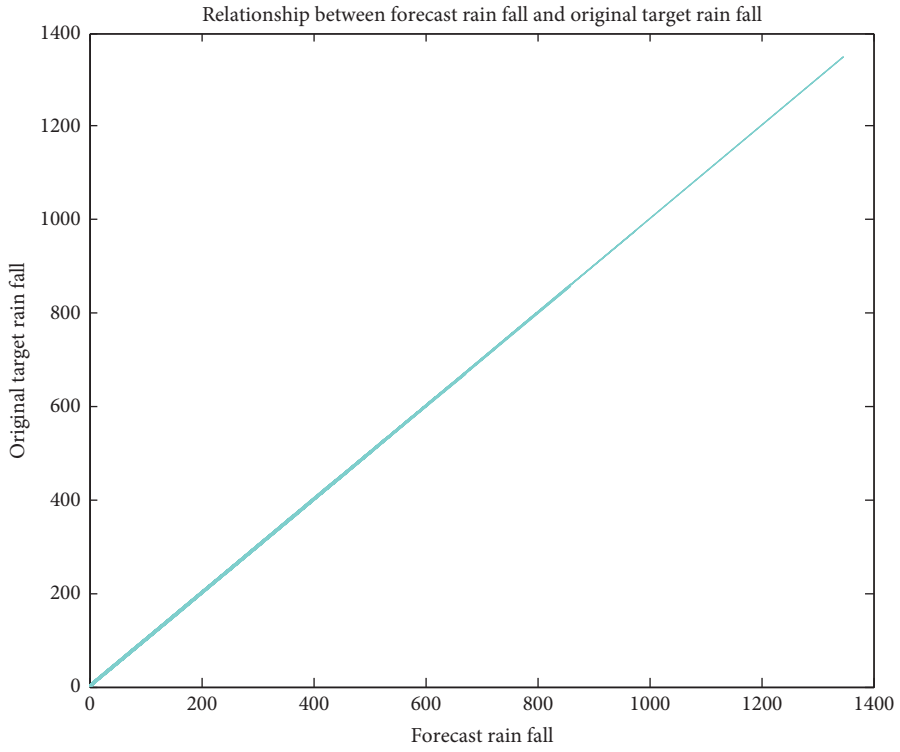

Figure 13: Relationship between forecast rainfall and original target rainfall.

The 11 hidden neurons associated with the single hidden layer Elman neural network forecast temperature match the target values. Hence, the error values are the least; it is clearly understood from Figures 15 and 16, respectively. The relationship between forecast temperature and the target temperature is linear; it is noticed from Figure 17.

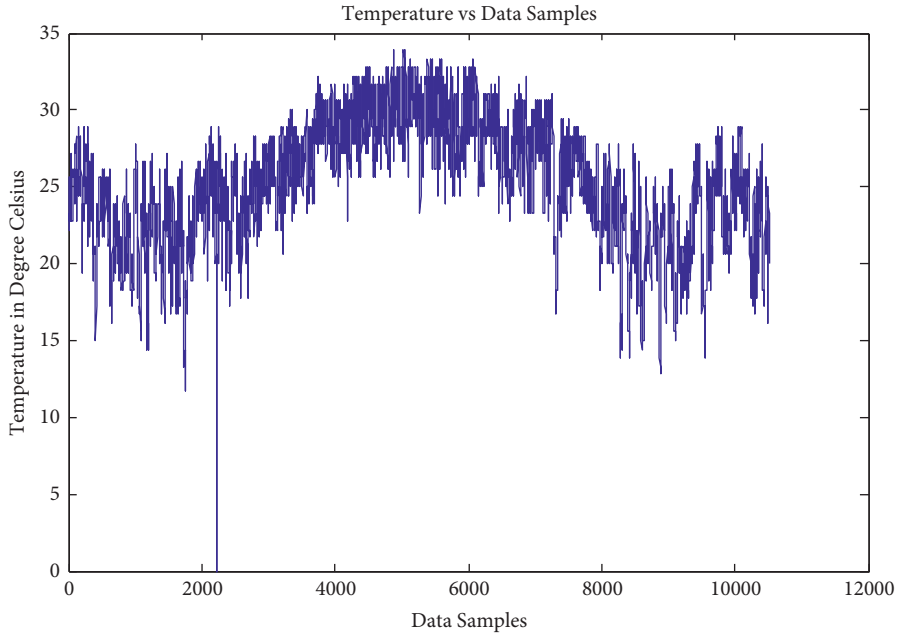

Figure 14: Temperature vs. data samples.

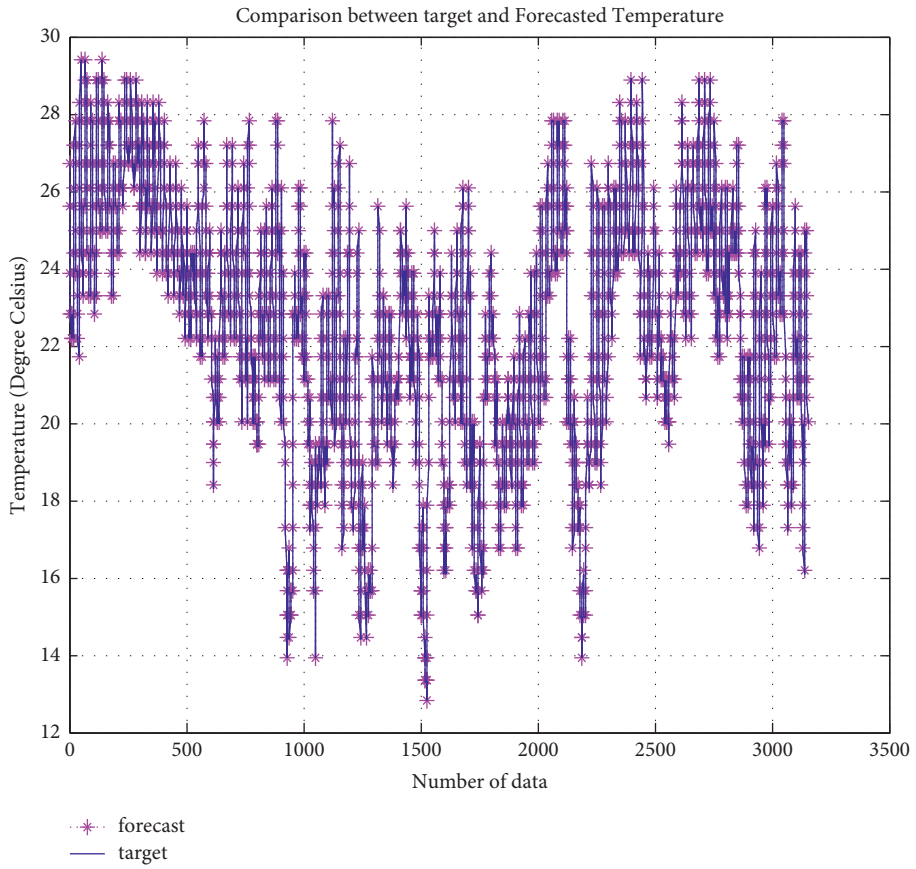

Figure 15: Comparison between target and forecasted temperature.

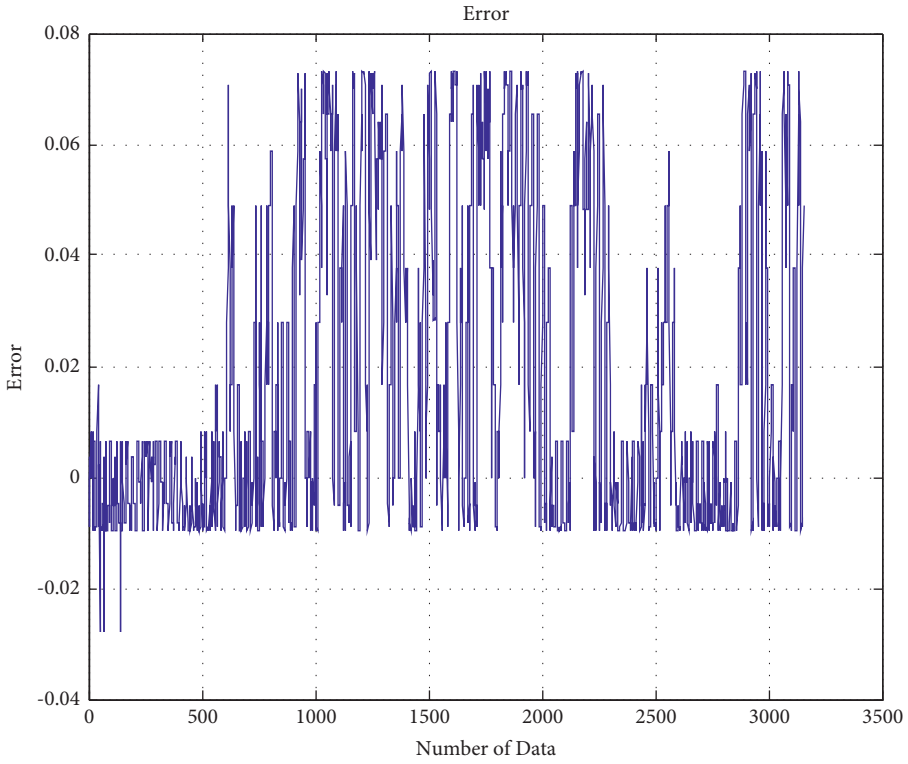

Figure 16: Error vs. number of data.

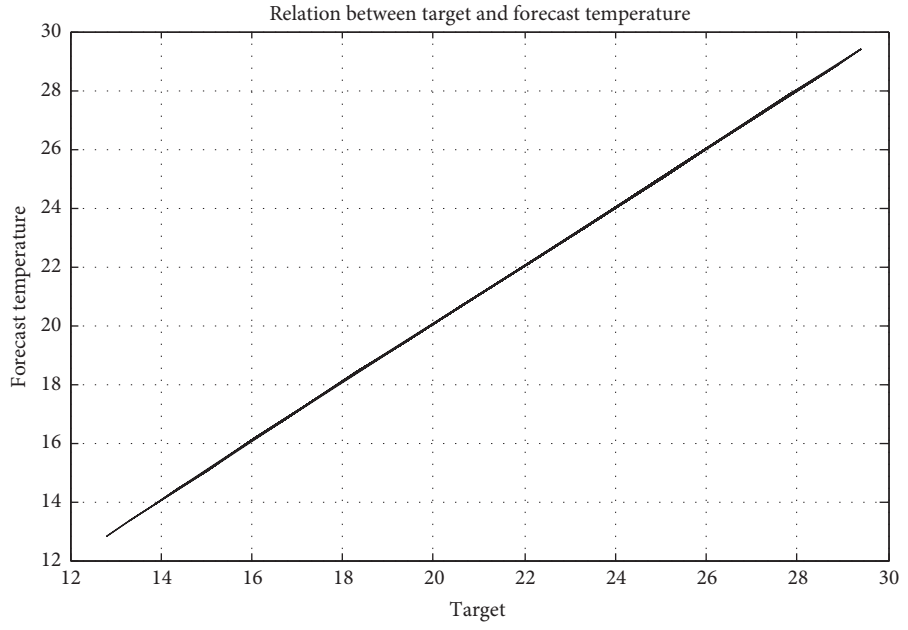

Figure 17: Relationship between target and forecast temperature.

5. Conclusion

Nowadays, human expectations and needs are increasing widely. All are interested in artificial intelligence to make their work easy and effective. This paper discusses the history of artificial neural networks, the generation of artificial neural networks, the generalized process involved in artificial neural networks, the various types, structural design, and artificial neural network applications that are elucidated in a detailed manner. The artificial neural network can address multiple applications, but this paper forecasting application is considered for performance analysis.

The highlights of the differences between the proposed models and the existing ones are as follows:

(i) The proposed models were developed with five years, five years, and seven years' data sets, respectively, for solar irradiance, rainfall, and temperature forecasting applications. Thus, we overcome the interannual variability-based uncertainty.

(ii) The proposed forecasting models possess minimal design complexity, are feasible to implement, and result in minor error qualifiers.

This paper proposed two feedforward neural networks, such as multilayer perceptron neural network (MLPNN) and improved backpropagation neural network (IBPNN), which could be used for forecasting applications like solar irradiance and rainfall forecasting, respectively. Moreover, the proposed one-feedback neural network, such as Elman neural network (ENN), can be used for the temperature forecasting application. The proposed artificial neural networks (MLPNN, IBPNN, and ENN) performances are statistically analyzed with various hidden neurons. The designed neural network–based forecasting model effectiveness is successfully validated using the acquired real-time training and test data set. Error qualifiers are used to analyze the performance of the proposed neural networks. According to the obtained results from the proposed artificial neural network–based forecasting model, it is observed that the proposed neural network–based forecasting model outperforms in all considered applications with much minimal error and reduced convergence time. The proposed multilayer perceptron neural network, which comprises 5 inputs, single hidden layer, and 14 hidden neurons achieves the minimal errors like $R = 1$, MAPE = 2.3034e-04, MSE = 5.9791e-07, MAE = 5.0093e-04, RMSE = 7.7324e-04, MRE = 2.3034e-06, and Time = 1.32 minutes for solar irradiance forecasting application. The suggested improved backpropagation neural network, which comprises five inputs, a single hidden layer, and seven hidden neurons, achieves minimal errors like $R = 1$, MAPE = 0.0158, MSE = 0.0042, MAE = 0.0320, RMSE = 0.0645, MRE = 1.5841e-04, and Time = 1.24 minutes for rainfall forecasting application. Similarly, the proposed Elman neural network, which comprises five inputs, a single hidden layer, and 11 hidden neurons, achieves minimal errors like MAPE = 0.1023, MSE = 0.0011, MAE = 0.0230, RMSE = 0.0332, MRE = 0.0010, and Time = 22 sec for temperature forecasting application. Hence, the proposed neural network–based forecasting models proved their validity, and they assist sustainability.

5.1. Proposed Forecasting Model Limitation and Future Work. To efficiently handle big data is one limitation of the proposed forecasting model. Thus, the authors can implement improved intelligent model-based forecasting in future work.

5.2. Recommendation of Future Direction and Research Scope. The building blocks of ANNs are neurons, linkages with weighted connection, activation function, and learning algorithms. Still, many research works focused on neural network performance improvement. The appropriated architecture selection was lacking in the field of artificial neural networks. There are no general guidelines available for the architecture framework. Artificial neural networks can effectively handle nonlinearity but obtain a feasible solution that is not generic. It can be overcome by the optimization algorithm associated with an artificial neural network (hybrid model). The readers can focus their research attention on the deep learning artificial neural network. However, ANN provided a promising result. Still, it has inefficiencies in some other applications like smart grid, natural language processing, speech recognition, computer vision, and so on, which lead to the quest to identify the optimal modeling of ANN.

The barrier to Growth in Artificial Neural Networks:

(i) Unique and privacy rights of the human being lost by an artificial neural network

(ii) Scarcity of job opportunities

(iii) Possibility to endanger humans and the environment

Artificial neural networks have many unique features and advantages; meanwhile, it has some barriers as well. Therefore, the advent of science and advancement should be healthy to benefit society, improve the economy and sustainability, and safeguard the environment and other living things.

Data Availability

We derived these data sets from the following domain resources https://www.noaa.gov/ upon request links to access their ordered data from an FTP site such as third-party right authors who did not provide the data openly.

Conflicts of Interest

The authors declare that they have no conflicts of interest.

Acknowledgments

The authors convey heartfelt thanks to the National Oceanic and Atmospheric Administration, the United States, for supporting real-time acquired data sample provision. Therefore, the authors validated the proposed research work successfully.

References

[1] F. Rosenblatt, "The Perceptron — a perceiving and recognizing automaton," Report 85–460–1, Cornell Aeronautical Laboratory, New York, NY, USA, 1957.

[2] K. Liu, X. Hu, J. Meng, J. M. Guerrero, and R. Teodorescu, "RUBoost-based ensemble machine learning for electrode quality classification in Li-ion battery manufacturing," *IEEE*, 2021.

[3] K. Liu, Z. Wei, Z. Yang, and L. Kang, "Mass load prediction for lithium-ion battery electrode clean production: a machine learning approach," *Journal of Cleaner Production*, vol. 289, Article ID 125159, 2021.

[4] K. Liu, X. Hu, H. Zhou, L. Tong, D. Widanalage, and J. Marco, "Feature analyses and modelling of lithium-ion batteries manufacturing based on random forest classification," *IEEE*, vol. 26, 2021.

[5] T. Hu, K. Li, H. Ma, H. Sun, and K. Liu, "Quantile forecast of renewable energy generation based on Indicator Gradient Descent and deep residual BiLSTM," *Control Engineering Practice*, vol. 114, Article ID 104863, 2021.

[6] X. Tang, K. Liu, K. Li, W. D. Widanage, and E. Kendrick, "Recovering large-scale battery aging data set with machine learning," *Patterns*, vol. 2, no. 8, Article ID 100302, 2021.

[7] K. Liu, Y. Shang, Q. Ouyang, and W. D. Widanage, "A data-driven approach with uncertainty quantification for predicting future capacities and remaining useful life of lithium-ion battery," *IEEE Transactions on Industrial Electronics*, vol. 68, no. 4, pp. 3170–3180, 2020.

[8] M. Madhiarasan and S. N. Deepa, "Determination of adequate hidden neurons in combo neural network using new formulation and fine tuning with IMGWOA for enrich wind-speed forecasting," *International Journal of Applied Research on Information Technology and Computing*, vol. 9, no. 1, pp. 89–101, 2018.

[9] M. Madhiarasan, L. Mohamed, and P. P. Roy, "Novel co-operative multi-input multilayer perceptron neural network performance analysis with application of solar irradiance forecasting," *International Journal of Photoenergy*, vol. 2021, pp. 1–24, Article ID 7238293, 2021.

[10] M. Madhiarasan and S. N. Deepa, "Long-Term wind speed forecasting using spiking neural network optimized by improved modified grey wolf optimization algorithm," *International Journal of Advanced Research*, vol. 4, no. 7, pp. 356–368, 2016.

[11] C. Lyu, S. Basumallik, S. Eftekharnejad, and C. Xu, "A data-driven solar irradiance forecasting model with minimum data," in *Proceedings of the IEEE Texas Power and Energy Conference (TPEC)*, pp. 1–6, IEEE, College Station, TX, USA, February 2021.

[12] J. I. Athavale, M. Yoda, and Y. Joshi, "Comparison of data driven modeling approaches for temperature prediction in data centers," *International Journal of Heat and Mass Transfer*, vol. 135, pp. 1039–1052, 2019.

[13] S. Manandhar, S. Dev, Y. H. Lee, Y. S. Meng, and S. Winkler, "A data-driven approach for accurate rainfall prediction," *IEEE Transactions on Geoscience and Remote Sensing*, vol. 57, no. 11, pp. 9323–9331, 2019.

[14] D. E. Rumelhart, G. E. Hinton, and J. L. McClelland, "A general framework for parallel distributed processing," in *Parallel Distributed Processing: Explorations in the Microstructure of Cognition*, pp. 45–76, MIT Press, Cambridge, MA, USA, 1986.

[15] W. McCulloch and W. Pitts, "A logical calculus of the ideas immanent in nervous activity," *Bulltin of Mathematical Biophysics*, vol. 7, pp. 115–133, 1943.

[16] D. O. Hebb, *The Organization of Behavior*, Wiley & Sons, New York, NY, USA, 1949.

[17] F. Rosenblatt, *Principles of Neurodynamics*, Spartan Books, Washington, DC, USA, 1962.

[18] B. Widrow and M. E. Hoff, "Adaptive switching circuits," *1960 IRE WESCON Convention Record*, pp. 96–104, 1960.

[19] B. Widrow, "Generalization and information storage in networks of Adaline' neurons," in *Self-Organizing Systems 1962*, M. C. Yovitz, G. T. Jacobi, and G. Goldstein, Eds., Article ID 435461, Spartan Books, Washington, DC, USA, 1962.

[20] L. A. Zadeh, "Fuzzy sets," *Information and Control*, vol. 8, pp. 338–353, 1965.

[21] J. J. Hopfield, "Neural networks and physical systems with emergent collective computational abilities," *Proceedings of the National Academy of Sciences of the USA*, vol. 79, no. 8, pp. 2554–2558, 1982.

[22] D. E. Rumelhart, G. R. Hinton, and R. J. Williams, "Learning internal representations by error propagation," in *PDP Research Group, Parallel Distributed Processing: Explorations in the Microstructure of Cognition (V1 and V2)*, D. E. Rumulhart and J. L. McClelland, Eds., vol. 1, MIT Press, Cambridge, MA, USA.

[23] L. O. Chua and L. Yang, "Cellular neural networks: theory," *IEEE Transactions on Circuits and Systems*, vol. 35, pp. 1257–1272, 1988.

[24] C. Cortes and V. N. Vapnik, "Support-vector networks," *Machine Learning*, vol. 20, no. 3, pp. 273–297, 1995.

[25] W. Gerstner and W. M. Kistler, *Spiking Neuron Models: Single Neurons, Populations, Plasticity*", Cambridge University Press, Cambridge, MA, 2002.

[26] G. E. Hinton, "A practical guide to training restricted Boltzmann machines," in *Neural Networks: Tricks of the Trade*, G. Montavon, G. B. Orr, and K. R. Müller, Eds., vol. 7700, Springer, Berlin, Germany, 2012.

[27] M. Madhiarasan and S. N. Deepa, "Comparative analysis on hidden neurons estimation in multi layer perceptron neural networks for wind speed forecasting," *Artificial Intelligence Review*, vol. 48, no. 4, pp. 449–471, 2017.

[28] M. Madhiarasan and S. N. Deepa, "A novel criterion to select hidden neuron numbers in improved backpropagation networks for wind speed forecasting," *Applied Intelligence*, vol. 44, no. 4, pp. 878–893, 2016.

[29] J. L. Elman, "Finding structure in time," *Cognitive Science*, vol. 14, no. 2, pp. 179–211, 1990.

[30] M. Madhiarasan and S. N. Deepa, "ELMAN neural network with modified grey wolf optimizer for enhanced wind speed forecasting," *Circuits and Systems*, vol. 7, no. 10, pp. 2975–2995, 2016.

[31] M. Madhiarasan and S. N. Deepa, "A novel method to select hidden neurons in ELMAN neural network for wind speed prediction application," *WSEAS Transactions on Power Systems*, vol. 13, pp. 13–30, 2018.

[32] M. Madhiarasan and S. N. Deepa, "Deep neural network using new training strategy based forecasting method for wind speed and solar irradiance forecast," *Middle-East Journal of Scientific Research*, vol. 24, no. 12, pp. 3730–3747, 2016.

[33] M. Madhiarasan and S. N. Deepa, "A new hybridized optimization algorithm to optimize echo state network for application in solar irradiance and wind speed forecasting," *World Applied Sciences Journal*, vol. 35, no. 4, pp. 596–614, 2017.

[34] M. Madhiarasan and S. N. Deepa, "Precisious estimation of solar irradiance by innovative neural network and identify exact hidden layer nodes through novel deciding standard," *Asian Journal of Research in Social Sciences and Humanities*, vol. 6, no. 12, pp. 951–974, 2016.

[35] J. Abbot and J. Marohasy, "Application of artificial neural networks to rainfall forecasting in queensland, Australia," *Advances in Atmospheric Sciences*, vol. 29, no. 4, pp. 717–730, 2012.

[36] G. Geetha and R. S. Selvaraj, "Prediction of monthly rainfall in Chennai using backpropagation neural network model," *International Journal of Engineering, Science and Technology*, vol. 3, no. 1, pp. 211–213, 2011.

[37] P. Zhang, Y. Jia, J. Gao, W. Song, and H. K. Leung, "Short-term rainfall forecasting using multilayer perceptron," *IEEE Transactions on Big Data*, vol. 6, no. 1, pp. 93–106, 2018.

[38] T. Cowan, M. C. Wheeler, O. Alves et al., "Forecasting the extreme rainfall, low temperatures, and strong winds associated with the northern Queensland floods of February 2019," *Weather and Climate*, vol. 26, Article ID 100232, 2019.

[39] A. Krzemień, "Fire risk prevention in underground coal gasification (UCG) within active mines: temperature forecast by means of mars models," *Energy*, vol. 170, pp. 777–790, 2019.

[40] B. Spencer, O. Alfandi, and F. Al-Obeidat, "Forecasting temperature in a smart home with segmented linear regression," *Procedia Computer Science*, vol. 155, pp. 511–518, 2019.

[41] M. Madhiarasan and S. N. Deepa, "Performance investigation of six artificial neural networks for different time scale wind speed forecasting in three wind farms of coimbatore region," *International Journal of Innovation and Scientific Research*, vol. 23, no. 2, pp. 380–411, 2016.

[42] M. Madhiarasan, "Accurate prediction of different forecast horizons wind speed using a recursive radial basis function neural network," *Protection and Control of Modern Power Systems*, vol. 5, no. 22, pp. 1–9, 2020.

[43] M. Madhiarasan, "Long-Term wind speed prediction using artificial neural network-based approaches," *AIMS Geosciences*, vol. 7, no. 4, pp. 542–552, 2021.

[44] M. Madhiarasan, M. Tipaldi, and P. Siano, "Analysis of artificial neural network performance based on influencing factors for temperature forecasting applications," *Journal of High Speed Networks*, vol. 26, no. 3, pp. 209–223, 2020.

[45] M. Madhiarasan, "Certain algebraic criteria for design of hybrid neural network models with applications in renewable energy forecasting," Ph. D. Thesis, Anna University, Chennai, India, 2018.

Hindawi
Journal of Electrical and Computer Engineering
Volume 2022, Article ID 5923568, 16 pages
https://doi.org/10.1155/2022/5923568

Research Article

Energy Management in the Microgrid and Its Optimal Planning for Supplying Wireless Charging Electric Vehicle

Salma Sraidi and Mohamed Maaroufi

Research Electric Energy and Command, Mohammadia Engineering School, Mohamed V University, Rabat, Morocco

Correspondence should be addressed to Salma Sraidi; salmasraidi@gmail.com

Received 30 September 2021; Revised 29 December 2021; Accepted 20 January 2022; Published 27 February 2022

Academic Editor: Mohamed Louzazni

The ongoing research work on electric vehicles (EVs) as well as the growing concern around the world to ensure a pollution-free environment is sure to lead to a significant increase in the number of EVs in the near future. The electrification of automobiles is an inevitable trend of future development. However, the growth of EVs relies on several elements: autonomy, the charging practice and infrastructure, the price, and the high amount of energy needed for supplying EV. This tendency impacts several points in transportation such as the road infrastructure and electrical power network. The aim of this article is the integration of new energy power sources as a part of the microgrid (MG) to supply EV with dynamic wireless charging. The main goal is to establish an energy management strategy reducing the running cost. The purpose is suggested for two kinds of operation mode: relying only on the MG (island mode) or relying on the MG and the large grid (grid-connected). The optimization problem is solved on the basis of the particle swarm optimization (PSO) algorithm. We could note that the stability of the microgrid in the off-grid mode is better, when the load is close to the output power of the distributed power supply. Through the coordination and cooperation of the battery output and the other two distributed power generation units, the microgrid can achieve its autonomy and maximize the economy of the system operation. Thanks to our methodology, a better revenue and an enhanced flexible dispatching of the system were met in the grid-connected mode as well.

1. Introduction

In recent years, EVs have been seen as a significant alternative to ensure faster energy transition and low-carbon footprint. It drew the attention of many researchers and manufactures. The electrification of automobiles is an expected movement for future development. However, EVs' autonomy and charging have always been an issue limiting their development. In a recent report [1], MIT states that the major challenge is to acquire an infrastructure for a nationwide charging of EVs rather than manufacturing batteries with affordable cost. Hence, in order to increase the penetration rate of EVs, countries are building large numbers of charging facilities connecting EVs to electric power system [2]. There are 57 charging stations in Morocco counting more than 92 connectors [3]. Currently, EV could be charged either by a regular cable or by a magnetic field as wireless charging. Wired charging stations are the most commonly used for EV energy supply from the grid [4]. These types of stations have many disadvantages. The battery charging requires plugging and unplugging under artificial inert conditions, which poses a safety hazard. On the other hand, the entire charging process requires manual operation with low automation. The wireless power transfer WPT technology [5, 6] uses a noncontact method for power transmission, which makes up for the shortcomings of the traditional direct contact power supply method and has many advantages.

The wireless charging could be static or dynamic; the static mode is proceeded when the vehicle is stopped, while in the other mode the EV is charged during the motion. The technic of dynamic wireless power transfer DWPT could be the sustainable solution needed for EV's integration on transportation systems. However, taking into account the

randomness of EV charging behaviour and assuming high penetration rate of EV, this solution represents some difficulties, with impacts on the infrastructures capacity and electrical network [7].

There have been numerous researches about the impact of EV charging on the grid in order to set an optimal recharging method, either by dimensioning an electrical charging station based on renewable energy [8] or by an integrated storage system as supercapacitor or batteries to reduce the peak demand [9]. The literature [10, 11] presented the conception of fast charging station based on renewable energies and storage systems would decrease the impact on the electrical network.

Renewable energy sources, such as solar, hydropower, and wind, have gradually evolved into the most developing fields in modern electrical engineering and technology [12]. However, the intermittent nature of photovoltaic (PV) and wind turbine (WT) power has brought some challenges with their integration into the local/large grid [13]. In addition, we may need to think about how to maximize the power generation efficiency of renewable energy and reduce the impact on the large power grid within the scope of affordable investment.

Compared with the traditional power grid, the MG integrates Distributed Power Sources (DPS) (as photovoltaic, wind, micro gas turbine, etc.), load, energy storage system, and control device to form an independent system. It could be independent or connected to the traditional power grid. Thus, the emergence of MGs related to RE could alleviate the conflict between large power grids and DPS. This minimizes the possibility of large power grids being damaged by DPS, as well as EV's large demand [14]. At present, there are three configurations to optimize energy storage: best index, optimal energy storage capacity, and system lowest cost [15]. Literature [16] proposes a model for the optimal operation of MGs, with the optimization goal of minimizing the total cost of the system, while meeting customer needs and system security. An efficient algorithm based on particle swarm optimization minimizes the total energy consumption and operating cost of the MG by optimizing the adjustment of control variables [17]. The integration of Bayesian network theory's advantage and particle swarm algorithm provides a new strategy for MG optimization operation based on Bayesian-particle swarm algorithm [18]. Literature [19] introduces an energy management strategy that is used in an independent solar-powered diesel-storage MG system and uses the enhanced Pareto evolutionary algorithm to calculate the optimal configuration of the capacity of each distributed unit. The energy management system (EMS) has an important role and benefit for the optimal management of MG [20]. Optimization, scheduling structures, and load shifting are the main EMS's challenges to deal with. Reference [21] presented a control method of demand response on smart grids and emphasized its utility and benefit for the smart grid. Based on a heuristic algorithm, an optimization and smart energy system for an MG related to EV permits reducing the cost of electricity for a population [22]. An investigation on the contribution of MG and EVs as key enablers for sustainable development shows that the integration of RE and management of EVs charging station all contribute to affordable and reliable energy system [23].

Microgrids can be a suitable energy supply for EV, with benefits on both the economic and environmental levels of the energy systems [24]. As a matter of fact, they can effectively mitigate the possible risks on the power grid that could be caused by large-scale charging of EVs [25]. MGs enable also the local consumption of energy which contributes actively in achieving "zero emission" objective [26]. To be environmentally friendly, the EVs should rely on a green energy supply in order to operate. Implementing wireless charging of EV and the new power generation into MGs will surely be beneficial for increasing EV popularity. Hence, the development of microgrids as a control strategy for EV wireless charging is crucial. Wider deployment of EV wireless charging along with new energy sources will certainly drive a higher capacity of new energy consumption.

On the basis of the previous discussions (role of MG, emergence of EV, and its impact on the electrical grid), this paper explores the necessity of MG energy management system for an efficient and stable operation. This MG intends to supply an electrified road dedicated to the DWPT. The paper also establishes an optimized dispatch suitable for a complementary wind-solar-storage system and puts forward the corresponding energy management strategy. To solve the optimization model, the PSO algorithm is used. In fact, the effectiveness and the accuracy of the optimization model and energy management strategy proposed in this paper are verified through calculation examples. Dynamic learning factors and inertia weights are applied to resolve the optimization problem with PSO algorithm. The strategy of EMS with the lowest running cost possible is carried out for two kinds of operation modes (island mode and grid-connected mode). Finally, the simulation analysis is achieved with two different load requirements by EV. The core of this paper is organized as follows: Section 2 presents the description of the studied system. Economic operation dispatch model of MG for both modes is detailed in Section 3. Section 4 covers the energy management strategy of the system and the choice of optimization model. The efficiency of the optimal scheduling model proposed was proved in Section 5 through a case study.

2. System Description

In view of the sustainable development and the turning point of energy generation, RE production is a crucial factor in the electricity generation system [27]. In addition, the massive integration of EV in the future would not only disturb the electrical network but also contribute to the pollution since it is supplied by the traditional thermal power plant [28]. Wind power and solar power are combined to form a wind-solar complementary system presenting a good solution [29]. Compared with solar or wind energy independent power supply systems, this complementarity is greatly enhanced. It effectively compensates for the utilization defects of wind or solar independent systems in terms of resources. The combination of solar-wind systems can achieve all-weather

power generation functions; also, it is equipped with energy storage devices to guarantee uninterrupted power supply [30].

Many researchers have developed diverse optimization models to deal with the EMS problem in MG especially linked to supplying a population [31], a smart home [32], or charging EV with regular cable in a traditional recharge station [33]. However, none of them have covered the subject of EV's dynamic wireless charging. Supplying the vehicle in-motion by DWPT offers the option of spreading the load along the road and therefore reducing the load power. The DWPT consists in directly feeding the engine; no physical linking is required between the grid and EV. The vehicle could be supplied any time on the day by passing across the electrified road without the necessity for stopping to recharge. This technic seems to be a sustainable solution to be combined in transportation systems to reduce carbon dioxide emissions in long distance rides.

Our system, as seen in Figure 1, proposes the integration of RE (solar and wind) to supply an electrified road destined to the wireless charging of EV. In addition, a storage device based on a battery is implemented in order to deal with the problem of solar and wind energies' intermittence. This system offers a reliable combination of MG technology and wireless power transmission technology for EV charging. Two modes would be studied:

(i) First mode: it consists of an isolated MG based on renewable energy sources along with a storage system, called island mode

(ii) Second mode: the same configuration of MG as the first mode is adopted; the only difference resides in its connection to the large grid, instead of being isolated

3. Economic Operation Dispatch Model of Microgrid

When the MG is operating on islands, it does not interact with the large grid. The total energy generated by the distributed power sources in the isolated MG is used for the operation of its own load within the MG. In this mode, wind power and PV power generation in the wind-solar hybrid MG is not dispatchable. At the same time, the MG is not connected to the electric energy of the large power grid, so the dispatching variables only exist in the storage system: the battery.

In grid-connected operation, the microgrid is connected to the external grid through a quick switch. Energy exchange between the larger grid and the MG is possible: selling and buying energy can be done in both directions, thus realizing the interaction between the MG and the grid. Both modes need to consider the coordination of the DPS's power output with the EV's demand. Nevertheless, the difference between the two operation modes is that the grid-connected one focuses on the interaction with the larger grid. The model proposed in this paper considers both off-grid and grid-connected modes and adopts a time-of-use tariff model in grid-connected mode, so that the system can have better revenue and more flexible dispatching methods.

3.1. Optimal Scheduling Model in the Island Operation Mode

3.1.1. Objective Function. This paper aims to establish an economic optimization model for the MG with the lowest operating cost 24 hours a day. In the island mode, the transaction of electric energy is stopped, and the MG is isolated from the large power grid. The optimization goal is shown in the following formula:

$$\begin{cases} \min M_{op} = \sum_{i=1}^{24} \left[C_{OM(pvi)} + C_{OM(wti)} + C_{OM(bat)} \right] + C_P \\ C_{OM(pvi)} = K_{OM_{pv}} * P_{pvi} \\ C_{OM(w\ di)} = K_{OM_{wt}} * P_{wti} \\ C_{OM(bati)} = K_{OM_{bat}} * P_{bati} \\ C_p = P_{vi} * k \end{cases} . \tag{1}$$

Here, M_{op} represents the operating cost of the MG in one day of operation, $C_{OM(pvi)}$ represents the operating cost of photovoltaic power generation equipment at the ith hour, $C_{OM(wti)}$ represents the operating cost of wind power equipment in the ith hour, $C_{OM(bati)}$ represents the operating cost of the battery storage system at the ith hour, K_{OM} is the operation and maintenance coefficient of each DPS where $K_{OM_{pv}} = K_{OM_{wt}} = 0.1095\ \$/Kw$ according to [34], and $K_{OM_{bat}} = 0.204\ \$/Kw$ according to [35]. C_p represents the penalty fee when there is a power shortage, P_{vi} is the load power shortage, and P_{pvi}, P_{wti}, and P_{bati} represent the output of photovoltaic power, wind energy, and battery at the ith hour. k is the penalty coefficient; its value is related to the unit price of electricity.

3.1.2. Constraints

(1) Distributed power output constraints:

$$\begin{cases} P_{pv_{min}} \le P_{pv} \le P_{pv_{max}} \\ P_{wt_{min}} \le P_{wt} \le P_{wt_{max}} \\ P_{bat_{min}} \le P_{bat} \le P_{bat_{max}} \end{cases} . \tag{2}$$

Here, P_{pv}, P_{wt}, and P_{bat} are the output power of PV power generation, WT power generation, and battery, respectively, and $P_{pv_{min}}$, $P_{wt_{min}}$, $P_{bat_{min}}$, $P_{pv_{max}}$, $P_{wt_{max}}$, and $P_{bat_{max}}$ are the upper and lower limits of PV power generation, WT power generation, and battery output power.

(2) Power balance constraints:

$$P_{vi} + P_{pvi} + P_{wti} + P_{bati} = P_{wpti}. \tag{3}$$

Here, P_{wpti} is the load demand for charging EV by WPT at the ith period.

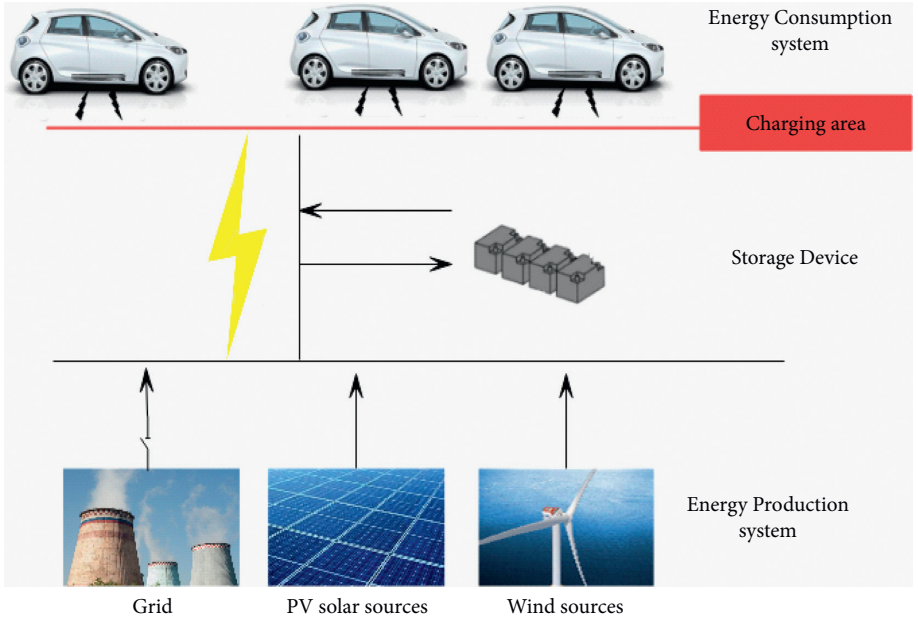

Figure 1: Production and consumption system.

3.2. Optimal Scheduling Model in the Grid-Connected Operation Mode

3.2.1. Objective Function. The fundamental factor that differentiates the MG connection from the isolated islands is the existence of electricity transactions. In addition, the amount of energy transactions is nonlinear. The minimum operating cost is taken as the optimization goal, as shown in the following equation:

$$\begin{cases} \min M_{op} = \sum_{i=1}^{24} \left[C_{OM(pvi)} + C_{OM(wti)} + C_{OM(bat)} + \left(M_{buyi} - M_{selli} \right) \right] + C_P \\ C_{OM(pvi)} = K_{OM} * P_{pvi} \\ C_{OM(wti)} = K_{OM} * P_{wti} \\ C_{OM(bati)} = K_{OM} * P_{bati} \\ C_p = P_{vi} * k \\ M_{buyi} = d * P_{buyi} \\ M_{selli} = h * P_{selli} \end{cases} . \tag{4}$$

Here, M_{buyi} means the cost of purchasing electricity from the grid at a given period *i*. P_{buyi} is the electricity purchased at that same period, and *d* is the electricity price, using the Time-of-Use (TOU) price model [36], as shown in Table 1. M_{selli} represents the income from electricity sales in the i^{th} period; P_{selli} is the electricity sold in the i^{th} period; *h* is the price coefficient of electricity sold, and the value in this paper is 0.29 $/kwh [37]; $P_{gri\ di}$ is the power exchanged with the large grid in the i^{th} period.

3.2.2. Constraints

(1) Distributed power output constraints:

$$\begin{cases} P_{pv_{min}} \le P_{pv} \le P_{pv_{max}} \\ P_{wt_{min}} \le P_{w\ d} \le P_{wt_{max}} \\ P_{bat_{min}} \le P_{bat} \le P_{bat_{max}} \\ P_{grid_{min}} \le P_{gri\ d} \le P_{grid_{max}} \end{cases} . \tag{5}$$

Here, $P_{grid_{min}}$ and $P_{grid_{max}}$, respectively, represent the minimum power and maximum power interacting with the large power grid.

(2) Power balance constraints:

$$P_{vi} + P_{pvi} + P_{wti} + P_{bati} + P_{gri\ di} = P_{wpti}. \tag{6}$$

Table 1: TOU price list.

Time period	Electricity price ($)
Peak time (11 h–17 h)	0.25
Normal time (23 h–7 h)	0.06
Valley time (7 h–11 h) (17 h–23 h)	0.1

Here, P_{grid} is the power value exchanged between the MG at the i^{th} period and the large grid, which is positive when purchasing electricity and negative when selling electricity.

4. Wind-Solar Complementary Microgrid Energy Dispatch Strategy

The core issue of energy management for MG is to optimize the output among power generation units. Therefore, this paper proposes an ideal dispatch strategy based on battery charge and discharge status to meet the requirements. Changing the charging and discharging state of the battery allows an optimal use of the released electric energy and at the same time ensures a proper operation of the system. In MG operation, there are two modes of operation: off-grid and grid-connected.

4.1. Off-Grid Operation Mode. According to the power generation data of PV and WT detected in the MG energy management system, the output of the battery is adjusted in a timely manner. The decision variable in this mode is the charge and discharge power of the battery. The sum of wind and solar outputs and the demand for the load of charging EVs have the three following situations:

(1) Wind and solar combined output cannot reach the EVs' load demand

(2) Wind and solar combined output equals the EVs' load demand

(3) Wind and solar combined output exceeds the EVs' load demand

When the first situation occurs, the battery is in discharge state, and the discharge amount is determined according to the electric energy shortage value. If the storage battery releases all the stored electric energy and still cannot meet the requirements, the power electronic devices inside the MG will act to reduce the power supply to EVs or give priority to EVs in need. As for the second situation, this is the most ideal state, the battery does not need to be charged or discharged. Meanwhile, in the third state, the battery stores electricity and could be used by the system in the first situation. If there is excess power after the battery is fully charged, this part of the energy is released into the Earth through the unloader, or it could be used in the road lightening.

4.2. Grid-Connected Operation Mode. There are also three situations for the magnitude of the combined wind and solar output and the demand on the load side:

(i) $P_{pv} + P_{wt} - P_{wpt} > 0$; the excess power charges the battery or can be sold directly to the large power grid. Due to the difference in electricity prices, we can choose to give priority to large grids when electricity prices are high in order to earn more revenue.

(ii) $P_{pv} + P_{wt} - P_{wpt} = 0$; neither charging or discharging the battery nor trading energy with the large power grid is possible.

(iii) $P_{pv} + P_{wt} - P_{wpt} < 0$; we choose either to discharge the battery or purchase electricity from the large grid. If the electricity price is high at this time, priority is given to using battery discharge to make up for the shortfall; otherwise, priority is given to purchasing electricity, and the electricity from the battery is reserved until the electricity price is high. The energy stored in the battery could be sold to the large grid in order to improve the economic benefits of the entire MG operation [34].

4.3. Application of PSO in Energy Management. Considering the problem and its size, we have adopted an optimization based on a heuristic algorithm. We assume that the PSO is suitable to verify and resolve the objective functions mentioned above.

The algorithm is an emerging optimization technology whose ideas are derived from artificial life and evolutionary computing theory. PSO completes the optimization by following the best solution found by the particles and the best solution of the entire group. It has been successfully used in function optimization such as system identification [38], neural network training [39], and other application fields.

The steps to apply PSO to the energy management of the MG start by searching a space identification and initializing PSO parameters, such as population size N, total number of iterations Max_{DT}, inertia weighting factors $\omega_{\min}$ and $\omega_{\max}$, and learning factors C1 and C2. The number of current iterations t is initialized at 0 $t = 0$. After that, we generate N random particle swarms. The initial position of each particle will be randomly set between the maximum and minimum of the control variable. Objective functions (1) and (4) are used to evaluate each particle in the initial population. For each particle swarm, $P_{\mathrm{besti}(0)} = X_{i(0)}$ is satisfied. Search for the optimal value of the objective function, and set the particles associated with the optimal value to the global optimal value $G_{\mathrm{besti}(0)}$. Set the initial value of the inertia weight to ω (0); the minimum and maximum values of the inertia weight factor are usually 0.4 and 0.9. All the steps are shown in Figure 2.

5. Case Study and Simulation

In order to evaluate if the suggested methodology is effective for enabling the integration of DPS on MG for charging electric vehicle with WPT, we opted for a load configuration taking into consideration real predictions of traffic on an hourly basis. This prediction used data collection of traffic

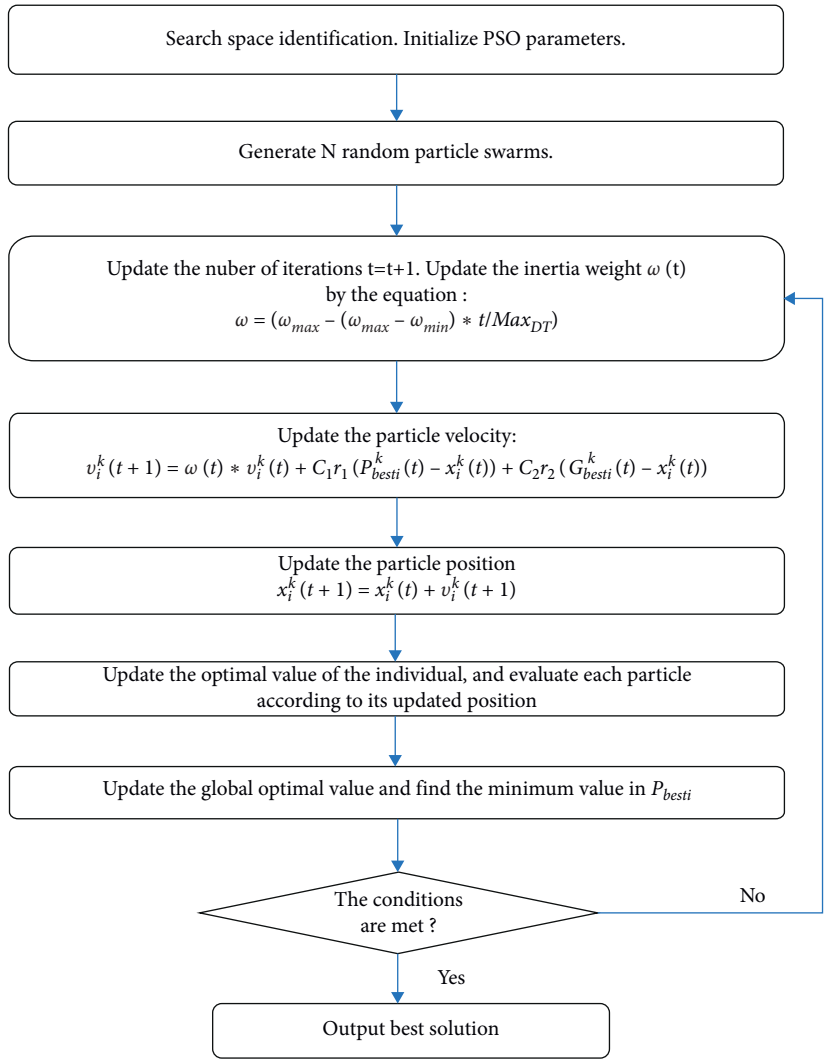

Figure 2: The steps of PSO.

flow of four-month span (January to April 2019), available on the Open Data Portal of Transport Infrastructure of Ireland [40].

The output power curve of the wind-solar hybrid unit derives from a biprobability-interval optimization model for wind-solar power day-ahead scheduling under uncertainties.

5.1. Load Profile. A lot of research has been done to predict the number of vehicles passing on a highway during a day. For our study, we were based on the curve given by the literature [40], which made a study of the traffic flow forecast hour-by-hour based on real data on the traffic in Dublin's metropolitan circle on seven highways.

It assumed a percentage of 1% of the vehicles which will be electrified and need to be recharged. The aim of the said study was to reestablish a pricing methodology for charging stations in areas rich in renewable energy. The curve of number of vehicles to be charged on highways hour-by-hour is given by Figure 3.

Different projects have tested the efficiency of WPT with different power transmission levels [41–43]. To evaluate the methodology and the optimization used in this paper, we consider 2 scenarios: the first one relies on an average power demand for each vehicle of 5 kW, while in the second one the average power demand is 15 kW as shown in Figure 4.

Figure 5 presents the demand of a single vehicle following the NEDC driving cycle [11]. As shown in this figure and from a microscopic standing point, EV load can create disturbance due to its inherently random load profile.

From a macroscopic point of view, if we consider the grid as the unique source of energy, as seen in Figure 4, the mobility energy needs peak coinciding with existing periods of grid loads peak. This situation is very detrimental to the electrical grid as it overloads it.

For these reasons, supplying the electrified road for WPT of EV by an MG based on RE would not only help with the zero emission but also help to avoid the impact on the electrical grid.

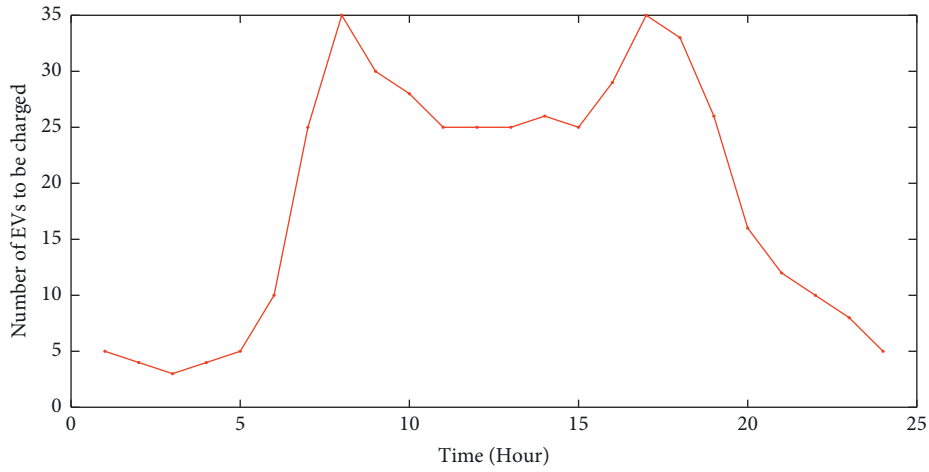

Figure 3: Number of EVs to be charged.

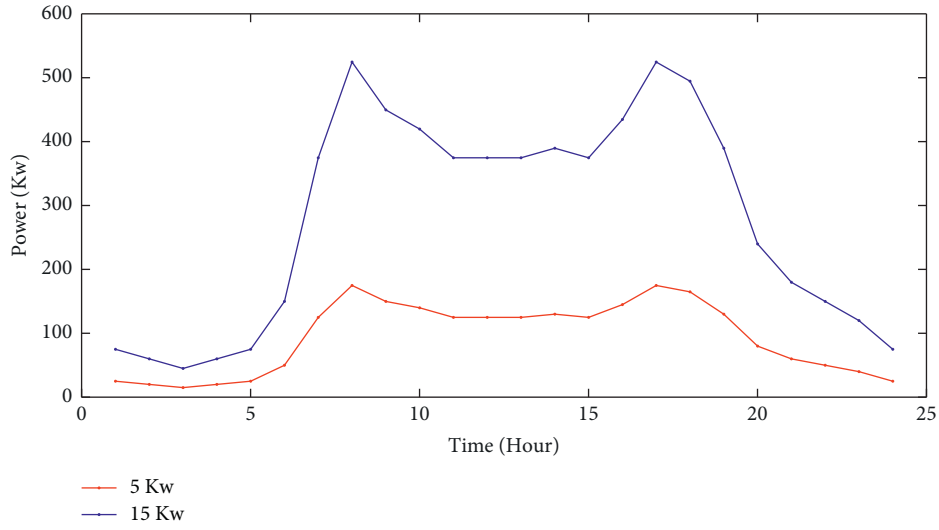

Figure 4: Load curves of EVs demand with an average power of 5 kW and 15 kW.

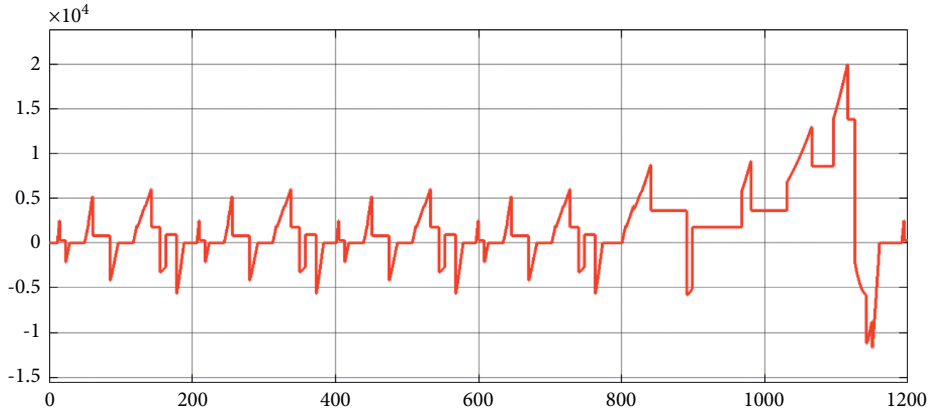

Figure 5: Power evolution as a function of time (s) for a single vehicle following NEDC cycle.

Subsequently, we would present the details of the charging EV by the isolated and grid-connected MG for different level of charge.

5.2. Island Mode. For our case, to study the electrification of road for the wireless power transfer of EV, we assume an output power curve of the wind-solar hybrid unit as shown in Figure 6 according to [44]; it was based on a biprobability-interval optimization model for wind-solar power day-ahead scheduling under uncertainties.

The upper limit of battery charging and discharging power is 150 kW, and the lower limit is 100 kW; we consider the power range of the interaction between the system and the grid as [−250 kW, 250 kW].

5.2.1. Charge 1: 5 kW. In the island particle swarm optimization algorithm, the maximum number of iterations is 300, and the number of particles is 600.

The optimized scheduling results show that the operating cost per day is 194.5 \$/day. If we consider that the electrified road was supplied directly from the grid, and using the TOU price shown in Table 1, the operating cost per day would be 360.8 \$/day, which gives us a daily gain of 166.3 \$ per day with the use of MG.

The output of each device is shown in Figure 7 and Figure 8.

Figure 6 presents the curve of the load considering that the average power demand of each vehicle is 5 kW and P_{re} presents the power output of the renewable energy installed in the microgrid as shown in the following equation:

$$P_{re} = P_{pv} + P_{wt}. \tag{10}$$

Figure 7 presents the shortage power or the power needed after feeding the demand by wind/solar power and the battery power output. As seen in this figure, the battery fills in the lack of power in the microgrid.

When there is little difference between wind/solar combined output and load demand, the optimized result is ideal. The effectiveness of optimization is explained by selecting two typical moments. When the wind and solar output is smaller than the required amount, it is sufficient to meet the demand of the load by discharging the battery. It can be clearly seen in Figure 9 that, at around 18 : 00 in the evening, the peak power demand of this day is ushered in. The combined solar and wind output can no longer meet the demand of the electrified road, and the difference is about 125 kW. Since the maximum discharge power of the battery selected in the MG system is 150 kW, it can completely make up for this part of the shortfall. Therefore, even in the evening when the load demand is large, there is no need to remove the load; thus the power supply reliability of the entire system is maintained. Similarly, at 5 o'clock in the morning, the combined solar and wind output at this time is greater than the required amount of electricity, with a difference of 29 kW. Since the upper limit power of the battery for charging has reached 100 kW, the extra energy can be absorbed by the battery itself, and the excess energy will not be wasted by leaking into the ground. The rest of the moments are also in the same situation as the above two moments. The battery can always discharge or store the power. From the definition in the objective function (1), it can be seen that the penalty fee for the last item is reduced to the lowest.

Under the premise of ensuring the reliability of power supply, the operating economy of the wind-solar complementary MG system is ensured.

5.2.2. Charge 2: 15 kW. The operating cost of the system is 3.09×10^3 \$/day. In the event of an important load demand of EVs or due to a huge power need in an electrified road destinated to the heavy-duty vehicles, the load profile may undergo a considerable change as shown in Figure 10. In short, the huge change in load will make the gap between it and the combined wind/solar output and load become larger and larger. By comparing Figure 11 and Figure 12, it can be clearly seen that the optimized result is not ideal due to the limitation of battery capacity, and the shortfall value after optimized scheduling is still relatively large. In this case, we could also select a typical moment to analyze the optimization results. At 8 o'clock in the morning, the difference reached as much as 483 kW. The maximum discharge power of the battery is only 100 kW, which is far insufficient to make up for the shortfall. At this time, the MG can adopt load shedding measures by assuming a methodology that requires feeding EVs with a state of charge in battery lower than 50% or reducing the average power to 10 kW or 5 kW, for example. However, the penalty cost for load shedding is quite expensive, and the operating cost has risen from 194.5 to 3099.7 \$. Under this circumstance, not only is the reliability of electricity usage not guaranteed, but also it brings huge losses to the entire power grid.

From the above analysis and research, it can be seen that when the load demand is close to the output power of the distributed power supply, the stability of the MG is better. Through the coordination and cooperation of the battery's output and the other two distributed power generation units, the self-sufficiency of the MG can be achieved. When there is a huge difference between the load demand and the output of DPS, the stability of the entire MG operation and the reliability of the power supply will become worse. Relying only on the supply and storage of batteries could not be useful under different load changes or to ensure the safety of the system, in addition to the economic impact. Therefore, in order to reduce a series of impacts brought by load changes, the next step will be to analyze the optimal scheduling of grid-connected operation modes.

5.3. Grid-Connected Mode

5.3.1. Charge 1: 5 kW. In the grid-connected operation model, there are two optimized variables: one is the charging and discharging power of the battery, and the other is the power interacting with the large grid. Therefore, the dimensions of the particle swarm optimization algorithm have become 48. The first 24 unknowns represent the magnitude of

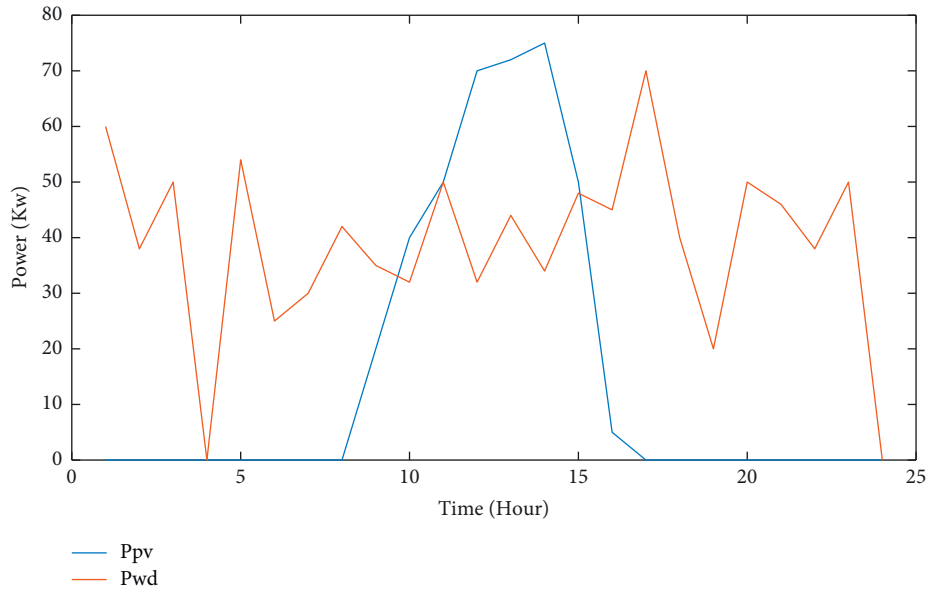

Figure 6: Output power curves PV/wind.

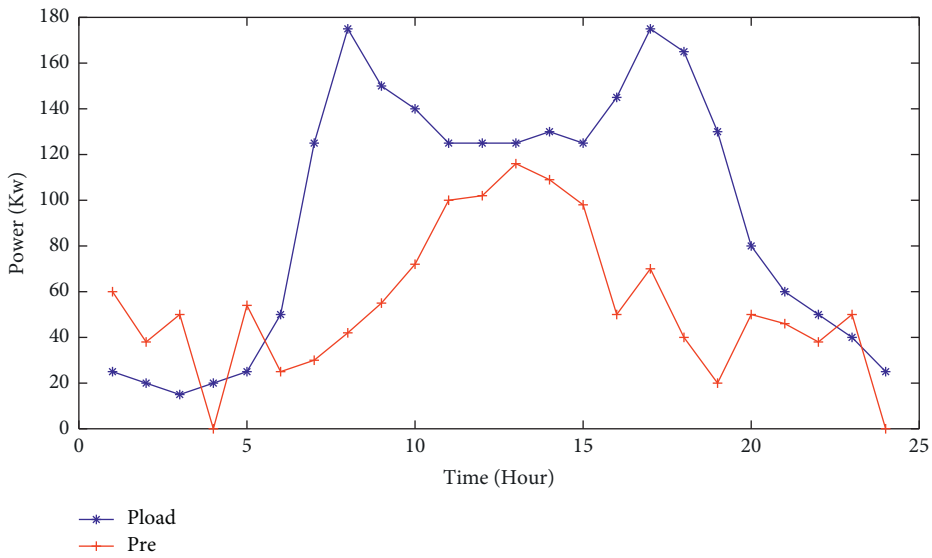

Figure 7: Comparison of wind-PV power output and load demand under the demand of 5 kW in island mode.

the interaction with the electric energy of the large power grid at each time in 24 hours, and the last 24 unknowns are allocated to the battery charging or discharging for each hour.

When the electricity price is changed, that is, when the TOU electricity price is adopted, the optimized results are shown in Figure 13 and Figure 14. It can be seen that, in this mode, it can still have good power supply reliability, but the charging and discharging of the battery and the transaction with the large power grid have undergone certain changes, which are caused by changes in electricity prices. At 10 o'clock, on the basis of ensuring the power consumption of the load, more power is sold to the large power grid through the battery discharge at 10 o'clock, and the load in the large power grid is relieved from the power supply pressure during the peak power consumption. More electricity is purchased in the parity stage from 23 to 7 hours and it is stored in batteries for use during peak electricity consumption. After the particle swarm optimization algorithm runs for one day, the income is about 253.4 $, which has better returns and a more flexible scheduling method than the model that does not use the Time-of-Use electricity price method.

5.3.2. Charge 2: 15 kW. When the super-large load shown in Figure 3 appears, the optimized results are shown in Figure 15 and Figure 16. When the electricity price is low, such as from 23 : 00 in the evening to 7 : 00 in the morning, it would be better to purchase electricity and store it in the battery power generation unit. In the time period from 16 :

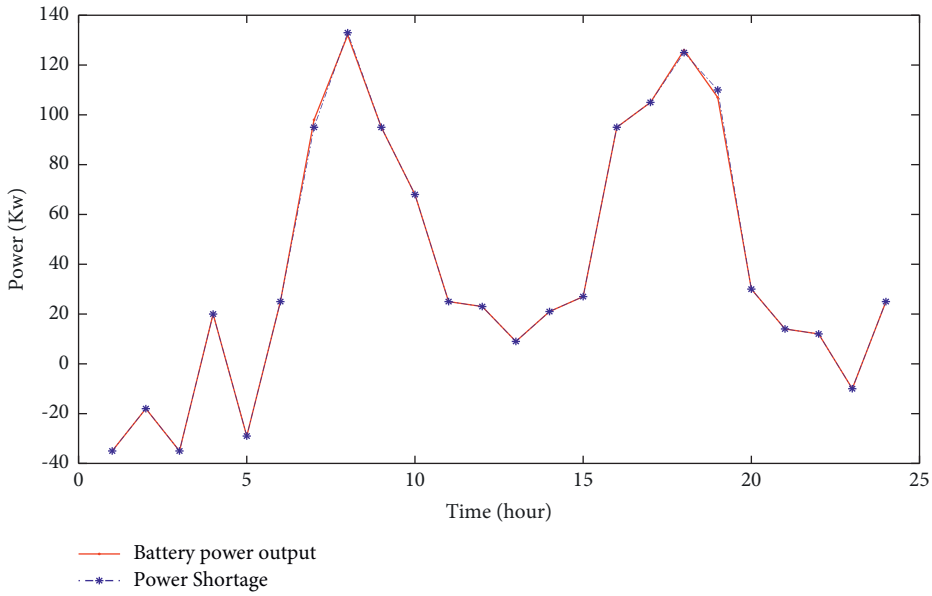

Figure 8: Battery output power and the shortage power under the demand of 5 kW in island mode.

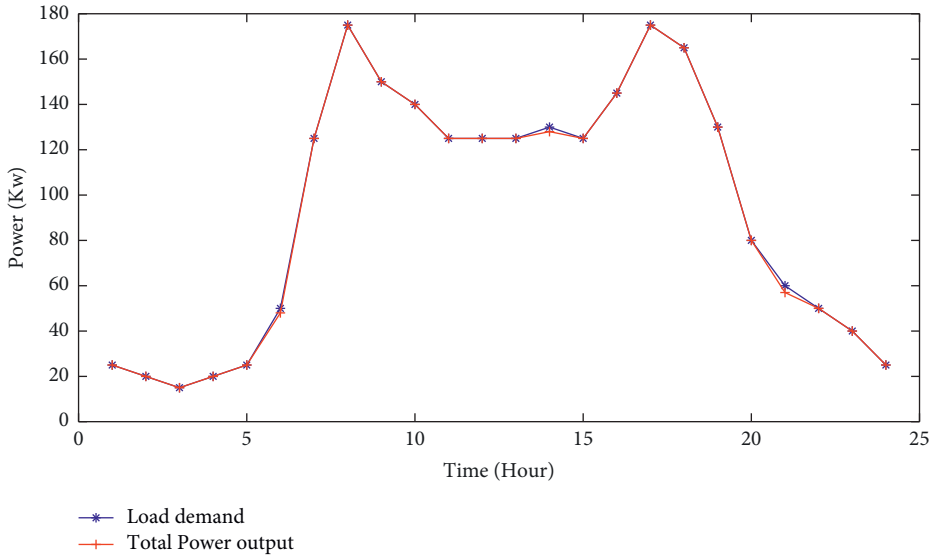

Figure 9: Load demand and total power supply under the demand of 5 kW in island mode.

00 to 19 : 00 and 8 : 00 in Figure 13, in order to give priority to ensuring the reliability of power supply, the battery discharge and power purchase have reached the upper limit, but the load demand is still not met, and penalty fees are incurred during this period. Despite the adoption of the Time-of-Use electricity price model, the operating cost on the last day reached 8372.9 $.

6. Discussion

Table 2 summarizes our results. In fact, if the electrified road was only powered by the electrical network, there will certainly be no power shortage. The network will be able to meet the need perfectly, but the price will be high. In addition, as previously discussed, such a demand would have a negative impact on the electricity network.

The suggested methodology would therefore make it possible to reduce the huge demand on the network. An example is shown in Table 2, in which two selected hours (8 a.m. and 7 p.m.) illustrate the importance of adopting an MG equipped with a suitable EMS in order to reduce the harmful impact of wireless charging on the electrical grid. We could see the power shortage, which is significant in the case of the huge load (15Kw per EV) in the off-grid mode.

Besides, when the load is close to the DPS's output power of the MG, there is no need to connect to the grid. The stability and autonomy of MG are ensured through the storage device.

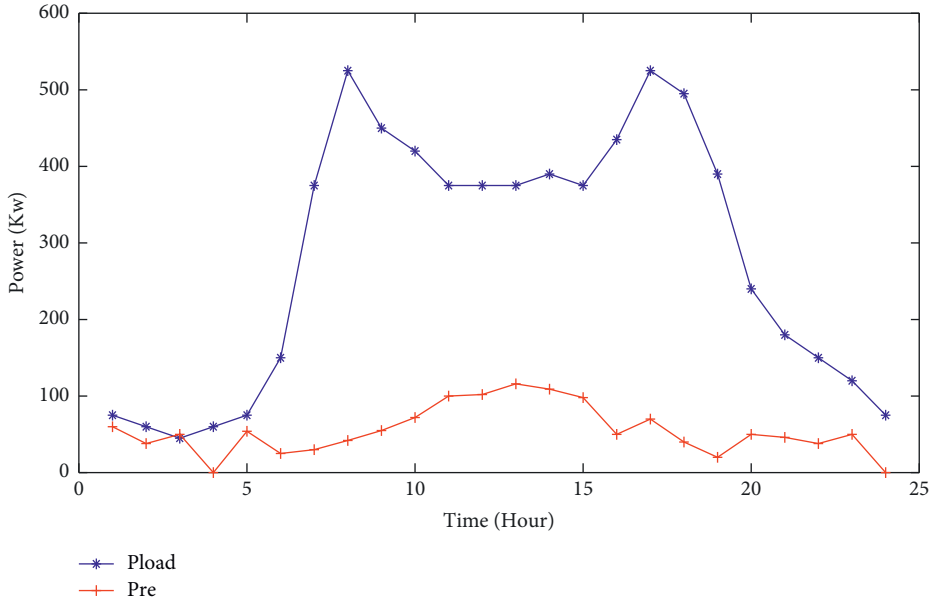

Figure 10: Comparison of MG output power and load demand by EV under the demand of 15 kW in island mode.

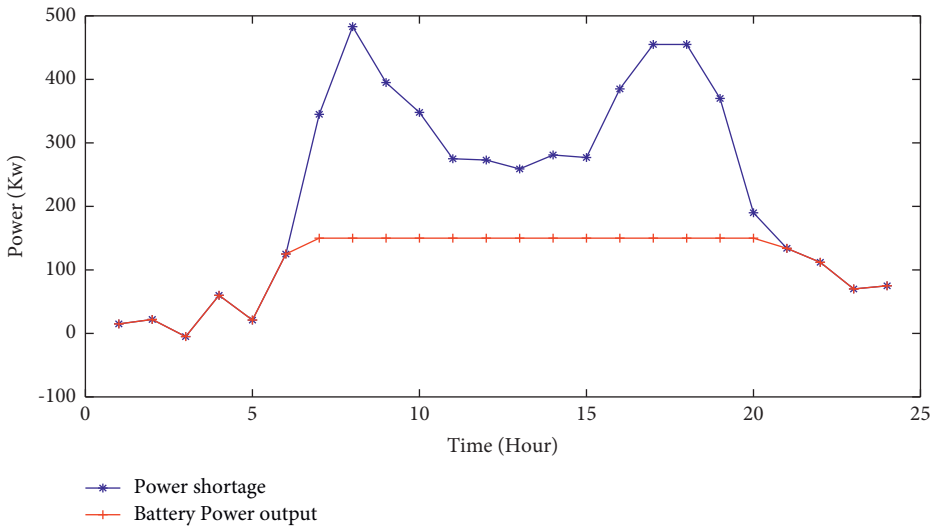

Figure 11: Comparison of battery output power and power vacancy under the demand of 15 kW in island mode.

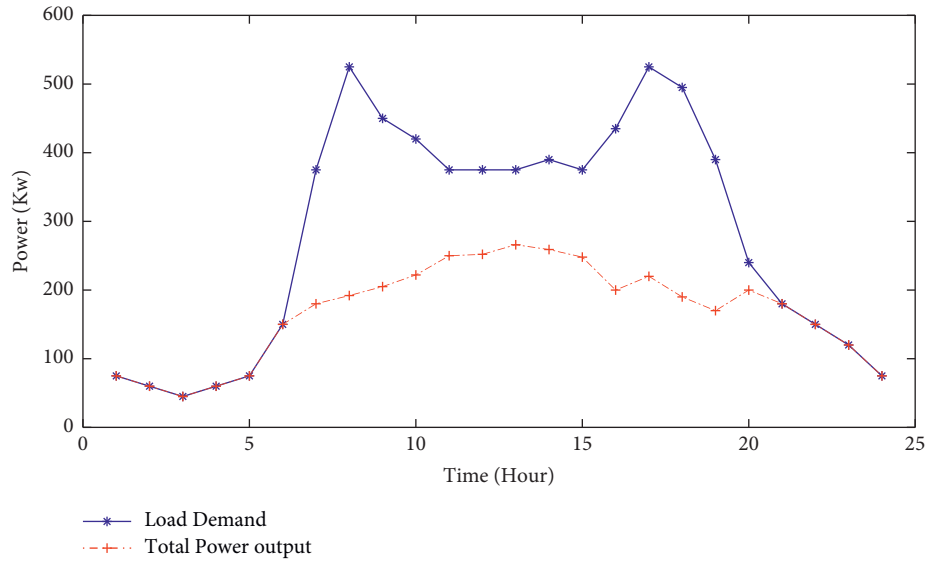

Figure 12: EVs load demand and total power supply under the demand of 15 kW in island mode.

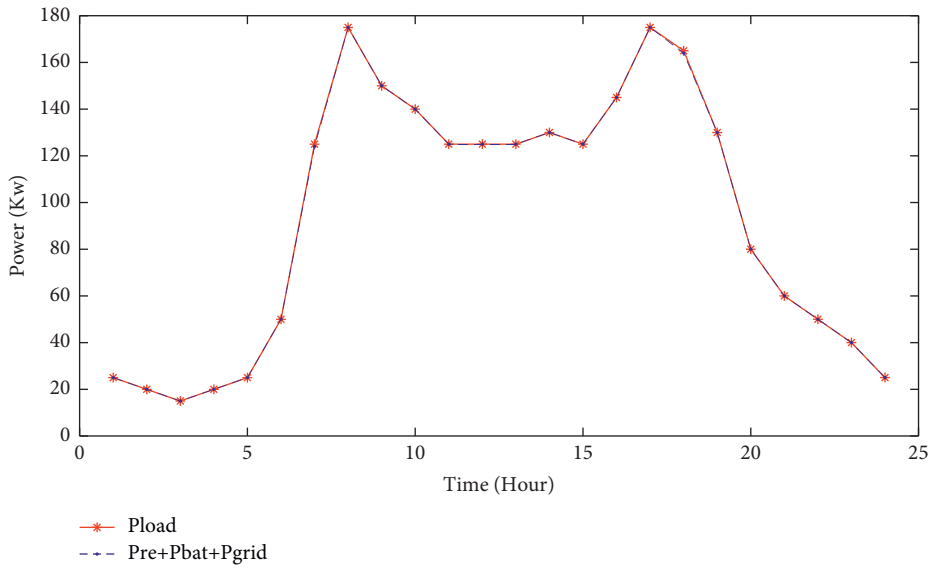

Figure 13: Load demand and total power supply under the demand of 5 kW in grid-connected mode.

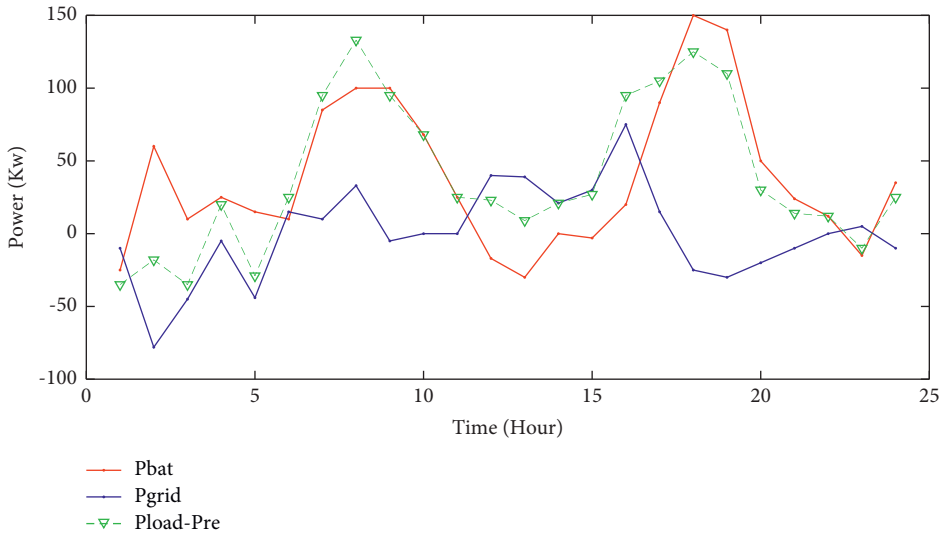

Figure 14: Battery output power and interaction energy under the demand of 5 kW in grid-connected mode.

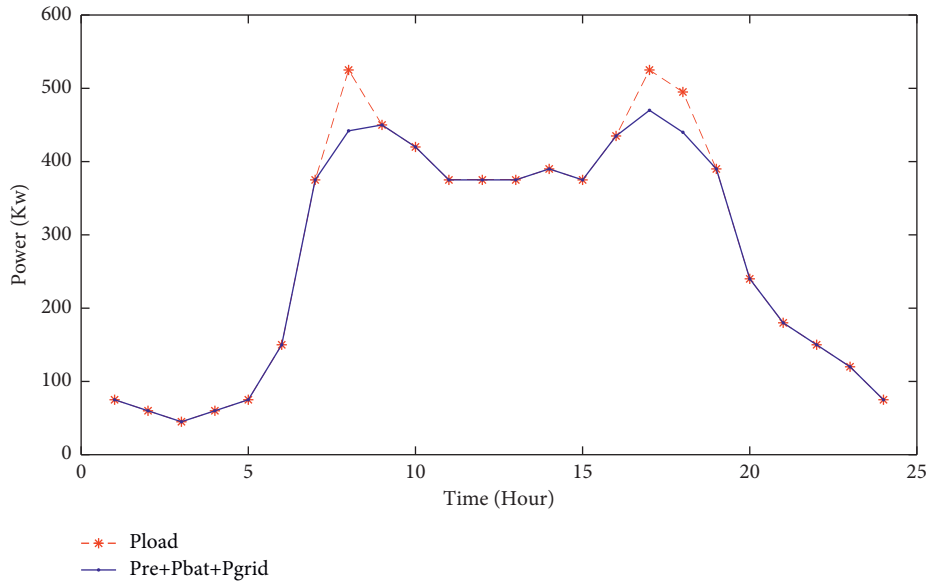

Figure 15: Load demand and total power supply under the demand of 15 kW in grid-connected mode.

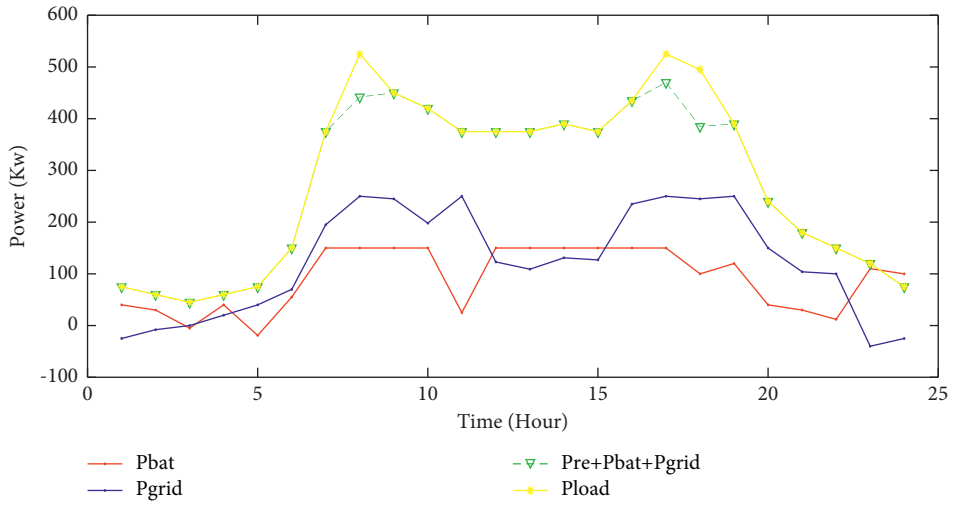

Figure 16: Battery output power and interaction energy under the demand of 15 kW in grid-connected mode.

Table 2: Result of feeding EV by WPT for a day.

Parameter	Unit	Off-grid mode		Grid-connected mode		Grid as a unique source	
		5 kW	15 kW	5 kW	15 kW	5 kW	15 kW
Load peak power	kW	175	550	175	550	175	550
Grid peak power	kW	—	—	75	250	175	550
Load demand at 8 a.m.	kW	175	525	175	525	175	525
Grid supply at 8 a.m.	kW	—	—	33	−30	175	525
Power shortage	kW	—	300	—	80	—	—
Load demand at 7 p.m.	kW	130	390	130	390	130	390
Grid supply at 7 p.m.	kW	—	—	250	250	130	390
Power shortage	kW	—	400	—	50	—	—
Charging cost	$	195	3099,7	253,4	8372,9	360,8	10965,3

Finally, thanks to the energy management system, the cost of the system is more viable in the case where the MG is implemented than when the grid presents the unique source supply.

7. Conclusions

Starting from the economic functioning of the MG and the necessity of feeding EVs, this paper has studied the optimal distribution model of the complementary wind-solar MG. Given the fact that this MG is supplying an electrified road for the dynamic wireless charging of EV under the modes of operation connected to the grid and isolated, the current paper proposes a corresponding energy management strategy. On this basis, an improved particle swarm optimization algorithm with dynamic weights and dynamic learning factors is proposed to give it better self-learning ability and better social cognitive ability. The actual calculation example shows that, in off-grid mode, when the load demanded by the vehicles is close to the output power of the distributed power supply, the stability of the MG is better. Through the coordination and cooperation of the battery output and the other two distributed power generation units, the MG can realize its self-sufficiency and maximize the economy of system operation. In the grid-connected mode, the Time-of-Use electricity price model is used to improve the system's revenue and dispatching methods flexibility.

Finally, this study could be further completed by an economic comparison of the various system's costs incurred due to a different choice of the optimization model (other than PSO).

Data Availability

All data used to support the findings of this study are included within the article.

Conflicts of Interest

The authors declare that there are no conflicts of interest.

References

[1] P. Behr, *MIT Panel says a charging infrastructure may be a bigger roadblock for electric vehicles than technology*, Scientific. American, 2011.

[2] H. S. Das, M. M. Rahman, S. Li, and C. W. Tan, "Electric vehicles standards, charging infrastructure, and impact on grid integration: a technological review," *Renewable and Sustainable Energy Reviews*, vol. 120, Article ID 109618, 2021.

[3] Electromaps, "Charge station at Morocco," 2021, https://www.electromaps.com/fr/station-de-recharge/morocco.

[4] L. Gan, U. Topcu, and S. H. Low, "Optimal decentralized protocol for electric vehicle charging," *IEEE Transactions on Power Systems*, vol. 28, no. 2, pp. 940–951, 2013.

[5] C. Panchal, S. Stegen, and J. Lu, "Review of static and dynamic wireless electric vehicle charging system," *Engineering Science and Technology, an International Journal*, vol. 21, no. 5, pp. 922–937, 2018.

[6] S. Niu, H. Xu, Z. Sun, Z. Y. Shao, and L. Jian, "The state-of-the-arts of wireless electric vehicle charging via magnetic resonance: principles, standards and core technologies," *Renewable and Sustainable Energy Reviews*, vol. 114, Article ID 109302, 2019.

[7] N. O. Kapustin and D. A. Grushevenko, "Long-term electric vehicles outlook and their potential impact on electric grid," *Energy Policy*, vol. 137, Article ID 111103, 2020.

[8] R. Mkhal, A. Nait-Sidi-Moh, and M. Wack, "Modeling and simulation of standalone photovoltaic charging stations for electric vehicles," *Int. J. Comput. Inf. Eng.*vol. 9, no. 1, pp. 72–80, 2015, https://waset.org/publications/10000396/modeling-and-simulation-of-standalone-photovoltaic-charging-stations-for-electric-vehicles.

[9] S. Salma, M. Mohamed, and E. L. A. Karim, "Ultracapacitor high power booster for dynamic wireless charging," in *Proceedings of the 2019 International Symposium on Advanced Electrical and Communication Technologies (ISAECT)*, pp. 1–7, IEEE, Rome, Italy, 27–29 Nov. 2019.

[10] J. A. Domínguez-Navarro, R. Dufo-López, J. M. Yusta-Loyo, J. S. Artal-Sevil, and J. L. Bernal-Agustín, "Design of an electric vehicle fast-charging station with integration of renewable energy and storage systems," *International Journal of Electrical Power & Energy Systems*, vol. 105, pp. 46–58, 2019.

[11] S. Sraidi and M. Maaroufi, "The role of distributed energy systems in electric vehicle wireless charging," in *Design, Analysis, and Applications of Renewable Energy Systems*, Elsevier, pp. 645–671, Amsterdam, Netherlands.

[12] H. Chen, C. Yang, K. Deng, N. Zhou, and H. Wu, "Multi-objective optimization of the hybrid wind/solar/fuel cell distributed generation system using Hammersley Sequence Sampling," *International Journal of Hydrogen Energy*, vol. 42, no. 12, pp. 7836–7846, 2017.

[13] S. Shivashankar, S. Mekhilef, H. Mokhlis, and M. Karimi, "Mitigating methods of power fluctuation of photovoltaic (PV) sources - a review," *Renewable and Sustainable Energy Reviews*, vol. 59, pp. 1170–1184, 2016.

[14] J. C. Vasquez, L. Tomislav, Q. Xiaonan, J. M. Guerrero, and M. Josep, "Aalborg universitet DC microgrids –Part II: a review of power Architectures, applications and standardization Dragicevic," *IEEE Transactions on Power Electronics*, vol. 31, no. 5, pp. 3528–3549, 2016.

[15] M. Faisal, M. A. Hannan, P. J. Ker, A. Hussain, M. B. Mansor, and F. Blaabjerg, "Review of energy storage system technologies in microgrid applications: Issues and challenges," *IEEE Access*, vol. 6, pp. 35143–35164, 2018.

[16] H. Hui Ren, A. Anwei Xiang, W. Weijun Teng, and R. Rongjia Cen, "Economic optimization with environmental cost for a microgrid," in *Proceedings of the 2012 IEEE Power and Energy Society General Meeting*, vol. 071003, pp. 1–6, IEEE, San Diego, CA, USA, 22-26 July 2012.

[17] A. T. Eseye, D. Zheng, J. Zhang, and D. Wei, "Optimal energy management strategy for an isolated industrial microgrid using a modified particle swarm optimization," in *Proceedings of the IEEE Int. Conf. Power Renew. Energy, ICPRE*, IEEE, Shanghai, Chinano, 21-23 Oct. 2016.

[18] Z. Zhuang, L. Qu, and X. Li, "Optimal operation of grid-connected microgrid based on particle swarm optimization," in *Proceedings of the Developments of Artificial Intelligence Technologies in Computation and Robotics: Proceedings of the 14th International FLINS Conference*, pp. 1350–1358, FLINS 2020, 2020.

[19] J. Zhao and X. Yuan, "Multi-objective optimization of stand-alone hybrid PV-wind-diesel-battery system using improved fruit fly optimization algorithm," *Soft Computing*, vol. 20, no. 7, pp. 2841–2853, 2016.

[20] M. Meliani, A. E. Barkany, I. E. Abbassi, A. M. Darcherif, and M. Mahmoudi, "Energy management in the smart grid: state-of-the-art and future trends," *International Journal of Engineering Business Management*, vol. 13, Article ID 184797902110329, 2021.

[21] M. Meliani, A. El Barkany, I. El Abbassi, A. M. Darcherif, and M. Mahmoudi, "Control system in the smart grid: state of the art and opportunities," in *Proceedings of the 2020 IEEE 13th International Colloquium of Logistics and Supply Chain Management (LOGISTIQUA)*, pp. 0–5, IEEE, Fez, Morocco, 2-4 Dec. 2020.

[22] F. Y. Melhem, O. Grunder, Z. Hammoudan, and N. Moubayed, "Optimization and energy management in smart home considering photovoltaic, wind, and battery storage system with integration of electric vehicles," *Canadian Journal of Electrical and Computer Engineering*, vol. 40, no. 2, pp. 128–138, 2017, http://ieeexplore.ieee.org.

[23] S. Bimenyimana, "Integration of microgrids and electric vehicle technologies in the national grid as the key enabler to the sustainable development for Rwanda," *International Journal of Photoenergy*, vol. 2021, Article ID 9928551, 2021.

[24] P. Mesarić and S. Krajcar, "Home demand side management integrated with electric vehicles and renewable energy sources," *Energy and Buildings*, vol. 108, pp. 1–9, 2015.

[25] M. Honarmand, A. Zakariazadeh, and S. Jadid, "Integrated scheduling of renewable generation and electric vehicles parking lot in a smart microgrid," *Energy Conversion and Management*, vol. 86, pp. 745–755, 2014.

[26] N. E. Koltsaklis, M. Giannakakis, and M. C. Georgiadis, "Optimal energy planning and scheduling of microgrids," *Chemical Engineering Research and Design*, vol. 131, pp. 318–332, 2018.

[27] I. Dincer, "Renewable energy and sustainable development: a crucial review," *Renewable and Sustainable Energy Reviews*, vol. 4, no. 2, pp. 157–175, 2000.

[28] W. Ke, S. Zhang, X. He, Y. Wu, and J. Hao, "Well-to-wheels energy consumption and emissions of electric vehicles: Mid-term implications from real-world features and air pollution control progress," *Applied Energy*, vol. 188, pp. 367–377, 2017.

[29] H. Zhang, Z. Lu, W. Hu, Y. Wang, L. Dong, and J. Zhang, "Coordinated optimal operation of hydro-wind-solar integrated systems," *Applied Energy*, vol. 242, pp. 883–896, 2019.

[30] M. Khalid, M. AlMuhaini, R. P. Aguilera, and A. V. Savkin, "Method for planning a wind-solar-battery hybrid power plant with optimal generation-demand matching," *IET Renewable Power Generation*, vol. 12, no. 15, pp. 1800–1806, 2018.

[31] M. Marzband, F. Azarinejadian, M. Savaghebi, and J. M. Guerrero, "An optimal energy management system for islanded microgrids based on multiperiod artificial bee colony

combined with Markov chain," *IEEE Syst. J.*vol. 11, no. 3, pp. 1712–1722, 2015.

[32] M. Marzband, H. Alavi, S. S. Ghazimirsaeid, H. Uppal, and T. Fernando, "Optimal energy management system based on stochastic approach for a home Microgrid with integrated responsive load demand and energy storage," *Sustainable Cities and Society*, vol. 28, pp. 256–264, 2017.

[33] Y. Zahraoui, I. Alhamrouni, S. Mekhilef et al., "Energy management system in microgrids: a Comprehensive review," *Sustainability*, vol. 13, no. 19, p. 10492, 2021.

[34] N. Nikmehr and S. Najafi-Ravadanegh, "Optimal operation of distributed generations in micro-grids under uncertainties in load and renewable power generation using heuristic algorithm," *IET Renewable Power Generation*, vol. 9, no. 8, pp. 982–990, 2015.

[35] T. Kerdphol, Y. Qudaih, and Y. Mitani, "Optimum battery energy storage system using PSO considering dynamic demand response for microgrids," *International Journal of Electrical Power & Energy Systems*, vol. 83, pp. 58–66, 2016.

[36] D. Kannan, "Time-of-use tariff and valley-filling based scheduling algorithm for electric vehicle charging," *Master Thesis, Institute of Architecture of Application Systems*, University of Stuttgart, Stuttgart, Germany, 2021.

[37] A. Zakariazadeh, S. Jadid, and P. Siano, "Integrated operation of electric vehicles and renewable generation in a smart distribution system," *Energy Conversion and Management*, vol. 89, pp. 99–110, 2015.

[38] B. Luitel and G. K. Venayagamoorthy, "Particle swarm optimization with quantum infusion for system identification," *Engineering Applications of Artificial Intelligence*, vol. 23, no. 5, pp. 635–649, 2010.

[39] M. Meissner, M. Schmuker, and G. Schneider, "Optimized Particle Swarm Optimization (OPSO) and its application to artificial neural network training," *BMC Bioinformatics*, vol. 7, no. 1, pp. 125–11, 2006.

[40] S. Zhou, "Dynamic EV charging pricing methodology for facilitating renewable energy with consideration of highway traffic flow," *IEEE Access*, vol. 8, pp. 13161–13178, 2019.

[41] S.-H. Lee and R. D. Lorenz, "Development and validation of model for 95%-efficiency 220-W wireless power transfer over a 30-cm air gap," *IEEE Transactions on Industry Applications*, vol. 47, no. 6, pp. 2495–2504, 2011.

[42] Y.-C. Hsieh, Z.-R. Lin, M.-C. Chen, H.-C. Hsieh, Y.-C. Liu, and H.-J. Chiu, "High-efficiency wireless power transfer system for electric vehicle applications," *IEEE Trans. Circuits Syst. II Express Briefs*, vol. 64, no. 8, pp. 942–946, 2016.

[43] S. Wang, J. Chen, Z. Hu, C. Rong, and M. Liu, "Optimisation design for series-series dynamic WPT system maintaining stable transfer power," *IET Power Electronics*, vol. 10, no. 9, pp. 987–995, 2017.

[44] J. J. Chen, Y. L. Zhao, K. Peng, and P. Z. Wu, "Optimal trade-off planning for wind-solar power day-ahead scheduling under uncertainties," *Energy*, vol. 141, pp. 1969–1981, 2017.